LITHOS 540–541 (2026) 108674

Contents lists available at ScienceDirect

LITHOS

journal homepage: www.elsevier.com/locate/lithos

High-temperature episyenites from late-Variscan Sàrrabus pluton (SE Sardinia, Italy)

F. Secchi [a,b], S. Naitza [c,d], A.M. Conte [b], G. Oggiano [a], M. Casalini [e], M. Kohút [f], T. Giovanardi [g,*]

[a] Dipartimento Scienze Chimiche, Fisiche, Matematiche e Naturali, Università degli Studi di Sassari, Via Piandanna 4, I-07100 Sassari, Italy
[b] IGAG - CNR - Sede Secondaria di Roma, c/o Dipartimento di Scienze della Terra, Sapienza Università di Roma, Roma, Italy
[c] Dipartimento Scienze Chimiche e Geologiche, Università degli Studi di Cagliari, Cittadella Universitaria S. S. 554 bivio per Sestu, I-09042 Monserrato, Cagliari, Italy
[d] IGAG - CNR - Sede Secondaria di Cagliari, c/o Dipartimento di Ingegneria Civile, Ambientale e Architettura, Università degli Studi di Cagliari, Cagliari, Italy
[e] Dipartimento Scienze della Terra, Università degli Studi di Firenze, Via La Pira 4, I-50121 Firenze, Italy
[f] Earth Science Institute, Slovak Academy of Sciences, Dúbravská cesta 9, Bratislava, Slovakia
[g] Dipartimento Scienze Chimiche e Geologiche, Università degli Studi di Modena e Reggio Emilia, Via G. Campi 103, I-41125 Modena, Italy

ARTICLE INFO

Keywords:
Na-metasomatism
Episyenite
Granodiorite
Late-Variscan shear zone

ABSTRACT

Uncommon high-temperature Na-metasomatized rocks close to sodic fenites are hosted in coeval granodiorites from the late-Variscan (286 ± 2 Ma) Sàrrabus pluton (SE Sardinia, Italy). They show sharp contacts with granodioritic host rocks and consist of small, irregular lenses of "spotted" rocks and hectometric layered, episyenitic bodies, scattered along a 15 km-long WNW trending extensional shear zone.

Alkali metasomatized rocks locally preserve the original textural and mineralogical features of granodiorites and display pervasive coarse grained recrystallization textures, with a wide range of mineral assemblages.

Spotted rocks display variably albitized plagioclase and anhedral K-feldspar, with interstitial aggregates of low-Ti diopside, partially or totally replaced by hastingsitic amphibole, producing the "spotted" macroscopic aspect. As the metasomatism becomes more pervasive, textures become xenomorphic or granoblastic, with low Ti-andraditic garnet coexisting with clinopyroxene close to aegirine-augite. Evolution of metasomatism is testified by dark mica + albite occurring as micro granoblastic aggregates along intergranular boundaries, and as chessboard albite replacing K-feldspar. Magnetite, titanite and apatite are ubiquitous accessory phases. Rare quartz with mortar textures occurs in veinlets and pegmatitic pockets.

Episyenites show εNd_{286} in the range of -6.29 to -6.78, overlapping the values observed for host granodiorites (-5.53 – -6.40). The $^{87}Sr/^{86}Sr_{286}$ ratio is in the range of 0.70922–0.71140, slightly higher than 0.70865–0.70969 of granodiorites. Petrographic evidence and the partially overlapped isotopic values suggest that episyenite originated from alkali metasomatism of a broad granodioritic protolith, caused by rock-interaction with Na-enriched, silica undersaturated fluids. Phase relationships for metasomatic systems and geo-thermo-oxybarometers calibrations constrain the *P–T–fO*$_2$ conditions at about 2.0 kbars, 450–750 °C, and -18.5 – -16.2, respectively.

Several stages of metasomatism occurred during the cooling of the granodioritic intrusion, leading to the formation of episyenite. These fault-controlled stages are linked to continuous variations in the fluids' physicochemical parameters, with *T* decreasing from near *solidus* to sub-*solidus* and hydrothermal conditions. Schematically, metasomatic stages may be summarized into: (1) *HT* albitization + primary biotite destabilization + Ca-silicate formation (diopside and andradite); (2) fluid-controlled metasomatic reactions leading to partial consumption of diopside and andradite with segregation of hastingsite, titanite and magnetite, and (3) final widespread albitization with hydrothermal hastingsite and, locally, dark mica and quartz precipitation. Overall, high-temperature processes resulted in a singular "sodic fenite" stage, with coarse recrystallization textures under near-solidus temperatures that overlaps those of magmatic stage. High temperature textures are then overlapped by lower temperature stages with a general increase in Na, fO_2 and aH_2O in the fluids, with a final and widespread albitization which may be interpreted as a true episyenitization stage.

* Corresponding author.
E-mail addresses: secchig@uniss.it (F. Secchi), snaitza@unica.it (S. Naitza), aidamaria.conte@cnr.it (A.M. Conte), giacoggi@uniss.it (G. Oggiano), martina.casalini@unifi.it (M. Casalini), milan.kohut@savba.sk (M. Kohút), tommaso.giovanardi@unimore.it (T. Giovanardi).

https://doi.org/10.1016/j.lithos.2026.108674
Received 13 November 2025; Received in revised form 8 June 2026; Accepted 9 June 2026
Available online 11 June 2026

1. Introduction

Episyenites are hydrothermally altered intrusive rocks commonly of broadly granitic composition occurring in the field as small bodies along fault zones and often associated with important ore deposits (e.g. Cuney et al., 2012; Petersson et al., 2014). Commonly, they post-dated the hosting intrusives and are schematically originated by dissolution of quartz by magmatic and/or meteoric fluids under brittle conditions of deformation. Solubility of quartz in aqueous fluids may increase with fluid alkalinity (Akinfiev and Diamond, 2009), and episyenitization is usually related to sodium metasomatism (Charoy and Pollard, 1989). However, quartz-depleted syenitic rocks are also found in alkali-metasomatized (fenitic) aureoles associated with alkaline and carbonatite intrusions (Le Bas, 2008). Fenites are characterized by metasomatic aegirine-augite (that may replace quartz) and alkali feldspar. While episyenitization typically results in a vuggy rock with variable hydrothermal cavity fillings, fenites may have undergone extensive recrystallization to the point where they resemble igneous syenites (Vartiainen and Woolley, 1976). In the Variscan orogen, high temperature episyenites resembling fenites, coeval to hosting granites, are described in central Iberian zone (Pérez-Soba and Villaseca, 2019).

In Sardinia, late Variscan granodiorites record both diachronous and coeval Na-metasomatic events along NE-trending fault zones, as also locally documented within the Sàrrabus pluton (Pirinu et al., 1996). In Sàrrabus pluton, however, due to the lack of an obvious fluid source and pervasively coarse recrystallization textures observed in these high temperature episyenites, their metasomatic origin is easily masked, and they may be misinterpreted as magmatic rocks (Brotzu et al., 1978; Pirinu et al., 1996).

In this paper, we discuss new petrographic, major, trace and isotopic data on whole rocks and minerals to constrain the processes leading to the formation of episyenite in the Sàrrabus pluton. Minerals major and trace elements have been used to estimate the geo-thermo-oxybarometers conditions of the episyenitization process, while U-Pb in situ analyses on titanite have been used to constrain its age, along with Ar-Ar and U-Pb dating of hosting intrusives. Whole rock analyses have been used to assess classification problems of metasomatic rocks, to determine the elemental budget of the metasomatic process through isocon models and to support a second age estimation. The whole data set suggests that episyenitization and high-temperature recrystallization may lead to formation of peculiar, distinctly metasomatic, episyenitic rocks. In a Variscan post-collisional context where the occurrence of granitoid was widespread, the network of strike-slip corridors, with locally associated extensional to transtensional shear zones, beside controlling the emplacement of many plutons played an important role in convoying fluids that account Na input at both high and low temperature (e.g. Petersson et al., 2014; Suikkanen and Rämö, 2019).

2. Geological setting

2.1. The Sardinia-Corsica Batolith

Sardinia island (Italy) represents a southern transect of the Variscan Belt intruded by many post-collisional coalescent plutons forming the Sardinia-Corsica Batholith (SCB; e.g. Carmignani et al., 1994). This plutonic-volcanic province emplaced through a complex succession of discontinuous short-lived magmatic episodes controlled by the activation of lithospheric shear zones (e.g. Casini et al., 2015a, 2015b; Cuccuru et al., 2016; Edel et al., 2014: Fig. 1a) during the late collisional and the post-collisional collapse of the Variscan orogeny and the exhumation of the orogenic roots. In this setting, lithospheric delamination and asthenospheric upwelling promoted the partial melting of the metaigneous and metasedimentary lower crust (Gaggero et al., 2017; Rossi et al., 2015; Secchi et al., 2022). As a result, a wide range of crustal melts, with subordinate mantle contribution, were produced (Cocherie et al., 1994; Conte et al., 2017; Macera et al., 2011; Rossi et al., 2015; Tommasini et al., 1995).

The formation of the SCB occurred during three stages: i) a 344–335 Ma late-collisional magmatic peak (Cocherie et al., 2005), documented in western and northwestern Corsica, ii) a Carboniferous post-collisional magmatic peak (from 322 ± 8 Ma in northern Sardinia, Casini et al., 2015a, to 299 ± 3 Ma in central Sardinia, Meloni et al., 2017), poorly represented in southern Sardinia (e.g. Burcei gabbrotonalites, 311 ± 9 Ma; Brotzu et al., 1993) and iii) a younger, Permian post-collisional magmatic peak (hereafter YMP, sensu Conte et al., 2017) widespread in Sardinia and Corsica (Casini et al., 2015a; Cocherie et al., 2005).

2.2. The Sàrrabus pluton

Geological and petrological aspects of Sàrrabus pluton were recently outlined by Secchi et al. (2021, 2022). The Sàrrabus pluton (400 km^2) is a multi-pulse, composite intrusive complex, emplaced at shallow crustal levels, in the frontal part of the orogenic wedge of the SE Sardinia. It records a complex evolutive history, consisting of several intrusive sequences mostly belonging to the YMP (Fig. 1). Schematically, the Sàrrabus pluton is a short-lived pluton emplaced in two main growth stages (Secchi et al., 2021, 2022).

Stage 1 occupies a large portion of the southern part of the pluton and consists of several pulses of granodiorites (Cala Regina Group in Fig. 1c). Particularly, the Cala Regina granodiorites, cropping out along the Sàrrabus southern coastline, represent a possible feeder zone. Evidence in favor of the feeder zone rooted in the southern part of pluton are in agreement with magnetic studies and Bouguer anomaly (Balia et al., 1989; Cassano et al., 1979). The southern portion of the Cala Regina Group features a 3 km wide WNW-trending belt hosting mingled magmas and dismembered gabbroic bodies within a foliated granodiorite rich in mafic enclaves aligned along the foliation. The mesoscopic features of the deformed bodies, according to the criteria in Paterson et al. (1998) suggest that the foliation was acquired under magmatic flow conditions. The WNW trending and steeply dipping (50° – 90°) foliation, the down deep lineation marked by the long axes of the deformed enclaves and megacrysts of plagioclase suggest the emplacement occurred within a dilatant normal shear. This normal shear was confined within an extensional stepover generated between two regional late Variscan strike-slip zones roughly oriented NS to NNW (Fig. 1a).

The heterogeneity of the magmatic products is typical of synplutonic shear zones that enhance magma mixing at depth and mingling at shallow level (Desouky et al., 1996) (Fig. 2a; b). As a consequence, the belt was regarded as a *syn*-plutonic shear zone (Southern Sarrabus Shear Zone; Secchi et al., 2021).

Stage 2 is a younger part made up of granitic rocks mainly widespread in the northern part of the pluton. This growth evolved northward with the emplacement of several suites of granites (Monte Maria and Bruncu Nicola Bove units) and F-bearing leucogranites that represent the end of intrusive magmatic activity (San Priamo and Monte Sette Fratelli units; Conte et al., 2017; Secchi et al., 2021, 2022).

The whole complex is extensively cut by several generations of mainly NNW-trending calcalkaline basic and acidic dykes. Remarkably, dense swarms of basic (spessartitic) dykes cut across the Cala Regina granodiorites and gradually decrease in frequency in the granitic units. They are associated with metaluminous acidic dykes and pre-date garnet-bearing peraluminous felsic dikes and satellite stocks.

A successive generation of olivine and plagioclase-bearing mafic dikes with tholeiitic signature, and aplites, crosscut the leucogranites and represents the end of Sàrrabus pluton igneous activity (Ronca et al., 1999; Secchi et al., 2021).

2.3. The episyenites

The use of the term ‘episyenite’ is thereafter preferred for the studied metasomatic rocks. This choice and classification aspects are treated in

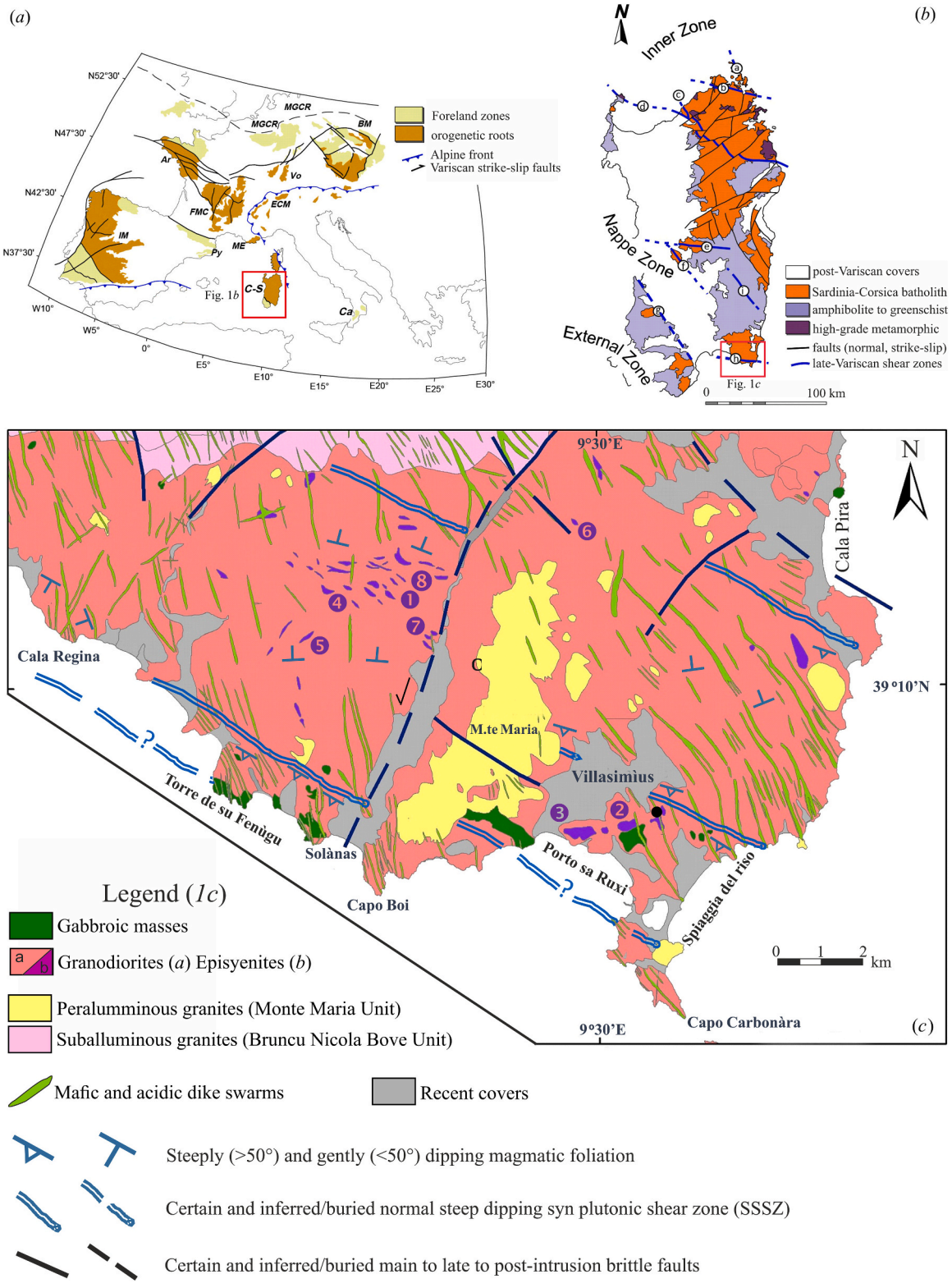

Fig. 1. (*a*) simplified geological map of Variscan massifs in Europe, modified from Martinez Catalan et al. (2021); IM – Central Iberian zoned, Py – Pyrenees, FMC – French Massif Central, Ar – Armorican Massif, ME – Maures-Esterel Massif, C-S – Corsica-Sardinia Massif, ECM – External Crystalline Massifs of the Alps, Vo – Vosges Massif, Ca – Calabria, MGCR – Mid-German Crystalline Raise, BM – Bohemian Massif; red box identifies the area of Fig. 1b; (*b*) Variscan units outcropping in Sardinia and associated shear zones: a-Isola Santa Maria 322 ± 8 Ma (Oggiano et al., 2007), b-Barrabisa 320–308 Ma (Casini et al., 2023), c-Badesi 300 ± 6 Ma (Oggiano et al., 2007), d-Posada-Asinara 325–300 Ma (Carosi et al., 2012), e-Mandrolisai 299 ± 3 (Meloni et al., 2017), f-Grighini 320–300 Ma (Secchi et al., 2022), g-Arbus 304 ± 4 Ma (Cuccuru et al., 2016) (h) SSSZ 285 ± 8 Ma (Secchi et al., 2021); red box identifies the area of Fig. 1c; (*c*) geological sketch map of late-Variscan southern Sàrrabus pluton (SE Sardinia, Italy). Simplified and modified after Secchi et al. (2021); distribution of albitized rocks, integrated after Brotzu et al. (1978) and Pirinu et al. (1996). ❶ to ❽ refer to Sedda sa Zarra, Campulongu, Cuccureddus, Cuccuru Ella, Marroccu, Minniminni, Nuraghes'Arridellaxiu and Bruncu Castangedda sampling localities, respectively. (For interpretation of the references to colour in this figure legend, the reader is referred to the web version of this article.)

the Discussion section.

The episyenites in the Sàrrabus pluton crop out discontinuously for at least 10 km mainly along a WNW-trending narrow belt as small outcrops hosted in granodiorites of Cala Regina group (Fig. 1c). The episyenite belt ends toward SE (Campu Longu sector; Fig. 1c), at the intersection with the Southern Sàrrabus Shear Zone, where in addition it is associated with gabbroic rocks (Fig. 1c).

In the field, episyenites occur as small and homogeneous or hectometric composite bodies. Small bodies, not exceeding few meters, consist of coarse-grained greenish colored spotted rocks defined as "leopard skin-like" by Pirinu et al. (1996), due to the occurrence of sub-centimetric clusters of clinopyroxene and/or amphibole (Fig. 2c). They form irregular lenses with sharp contacts (Fig. 2c; d) or fill sub-vertical or irregular fractures in granodiorites. Remarkably, they may contain microgranular dark enclaves disposed along the general magmatic foliation recorded in granodiorites (Fig. 2c).

Composite bodies occur as discrete stocks at the top of granodioritic intrusion, hosted in porphyritic border facies (e.g. Sedda sa Zarra, Cuccuru Ella outcrops) or equigranular rock-types, from which they are commonly separated by a gently deepening sharp contact. They schematically show a sub-horizontal banded structure roughly parallel to magmatic foliation of granodiorites, with bands where spotted rocks are inhomogeneously replaced by albite-rich, roughly layered rocks, and bands of true albitites (Fig. 2e). Locally (Sedda Sa Zarra) they also include aplo-pegmatite veins associated with a stockwork of thin quartz veins (Fig. 2f). According to Pirinu et al. (1996), late-veining is confined to episyenites.

Episyenites do not cut across the Monte Maria peraluminous leucogranites (Stage 2) and are crosscutted by spessartite dikes. A published Rb/Sr whole rock isochron based on 4 episyenite samples indicates an age of 294 ± 9 Ma (Pirinu et al., 1996) which overlaps, within the correlate error, to the age of 286 ± 15 Ma obtained by Laser Ablation-Inductively Coupled Plasma-Mass Spectrometry (LA-ICP-MS) U/Pb on zircons for hosting coeval granodiorites of Stage 1 (Secchi et al., 2021).

3. Analytical methods

Chemical and isotopic composition of rocks and main mineral phases was determined to complete the dataset reported in Pirinu (1994) and Pirinu et al. (1996) for mainland outcrops, and Brotzu et al. (1978) for Campu Longu outcrops.

Chemical composition of main mineral phases was determined at the

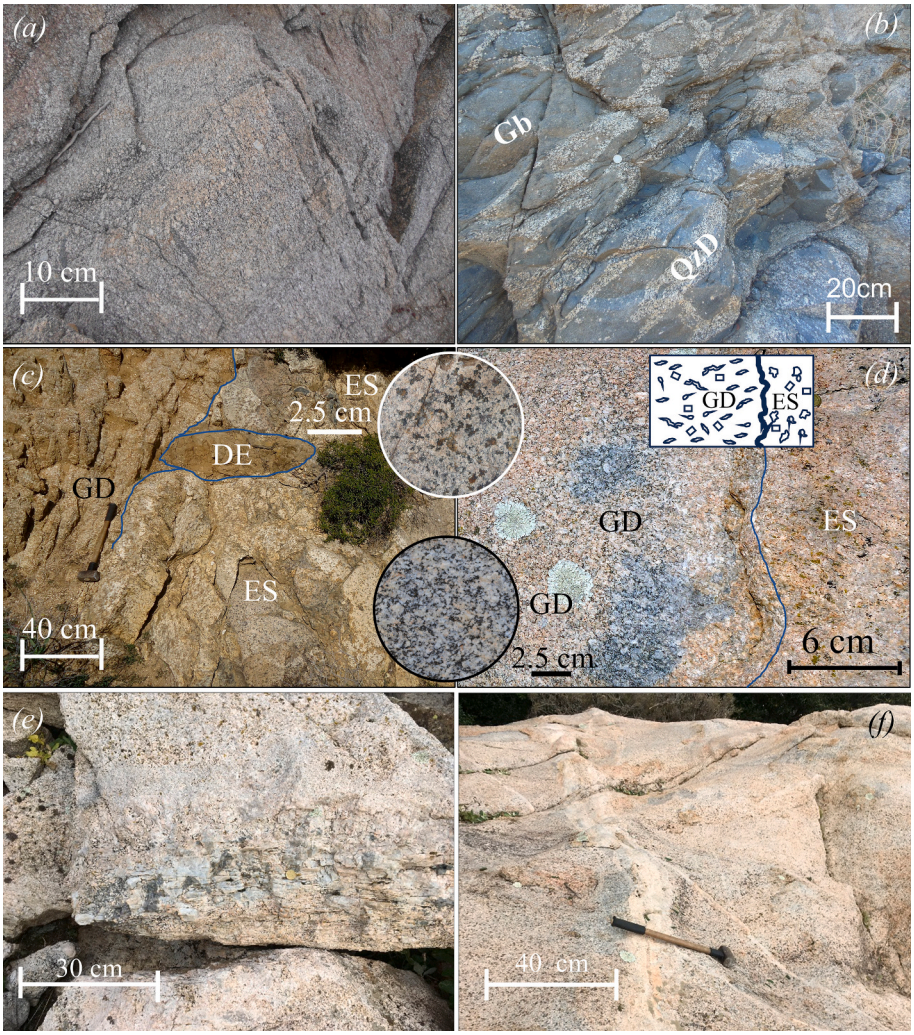

Fig. 2. Field aspects of locally altered episyenites from late-Variscan Sàrrabus pluton: (*a*) Field aspects of SSSZ. Deep steeply foliation of granodiorites (Solanas); (*b*) Field aspects of SSSZ. Swarm of hornblende micro gabbroic enclaves (Gb) densely dispersed into hosting granodiorite (GD; Solànas); (*c*) Examples of sharp contact between granodiorites (GD) containing flattened albitized dark enclave (DE) and spotted episyenite (EP) from homogeneous body (sample SSP37; Marroccu); (*d*) Spotted episyenitic rocks (EP) filling irregular network of fractures in altered granodiorites (Bruncu Nuraxeddu); (*e*) Rough layering displayed by aplo pegmatitic sub-horizontal albitite bands in Sedda sa Zarra composite body; (*f*) Sub-vertical continuous hololeucocratic decimetric and centimetric veins crosscutting spotted albitites in Sedda sa Zarra composite body.

Istituto di Geologia Ambientale e Geoingegneria - Consiglio Nazionale delle Ricerche (IGAG-CNR) laboratory in Rome, Italy, using polished carbon-coated mounts and a 4 spectrometer Cameca SX50–52 electron microprobe (EMP) instrument. In situ measurements were performed at 15 keV accelerating voltage, 15 nA beam current, and 10 s counting time per element. Analyses were calibrated using the following natural and synthetic standards: orthoclase (K), wollastonite (Ca, Si), native manganese (Mn), corundum (Al), jadeite (Na), magnetite (Fe), native nickel (Ni), potassium chloride (Cl), periclase (Mg), native chromium (Cr), rutile (Ti), silvite (Cl) and fluorophlogopite (F). In these operating conditions, the detection limit is between 30 and 100 ppm. We decided to consider the 100 ppm limit to be conservative. Full correction for atomic number effect, X-ray absorption and X-ray fluorescence (by characteristic and continuum excitation) were based on a Pouchou and Pichoir's (1991) procedure (PAP procedure). Data are reported in Supplementary Material from Table S1 to Table S7.

Whole-rock major and trace element concentrations of twelve samples representing the different Sàrrabus lithologies were determined at Activation Laboratories, Ltd. 164 (ACTLABS). Powdered samples were previously fused using lithium metaborate or tetraborate, and then rapidly digested in weak nitric acid solutions. Resulting solutions were analysed by inductively coupled plasma–optical emission spectroscopy (ICP–OES) and ICP–mass spectrometry (ICP–MS) techniques. The uncertainties in major element concentrations are generally between 1% and 3%, except for MnO (5%–10%) and P_2O_5 (>10%); most trace element concentrations have uncertainties of <5%. Major element concentrations usually have detection limits of 0.01 wt%. Loss on ignition (L.O.I.) and FeO contents were measured using standard gravimetric techniques and titration with 10 N $KMnO_4$ techniques, respectively. Data are reported in Supplementary Material Table S8.

A representative sample (PEG M SEDDAS) of episyenite from Sedda sa Zarra (1 in Fig. 1) was selected for in situ U/Pb titanite dating to compare with previously published U/Pb zircon ages from hosting granodiorites by Secchi et al. (2021). Titanites were analysed in a 100-μm thick polished thin section. U/Pb isotopes were determined using a iCAP-TQ ICP-MS (ThermoFisherScientific) coupled to a 213 nmNd:YAG laser ablation system (NewWave Research™) at the laboratories of the Centro Interdipartimentale Grandi Strumenti of the Università di Modena e Reggio Emilia using a spot of 55 μm and a fluence of 6.7 J/cm^2. U-Pb ratios were corrected for laser-induced elemental fractionation using an in-house Excel spreadsheet and titanite reference material OLT-1 (literature accepted values from Ma et al., 2019) which was analysed during the analytical session every 5 unknown analyses. Data were then treated using the on-line IsoplotR software (Vermeesch, 2018). Elemental concentrations were calculated using the method of Longerich et al. (1996). ^{44}Ca was measured during the analytical session and used as an internal standard considering a 27 wt% of CaO from the stoichiometric formula of titanite. Reference material NIST 612 was used as an external standard. Data is reported in Supplementary Material Table S9.

Nine episyenite selected samples were analysed for Sr and Nd isotopic compositions at the laboratories of Dipartimento Scienze della Terra of the Università degli Studi di Firenze (Italy). Sr and Nd measurements were obtained by a Thermofisher Triton Plus multi-collector mass-spectrometer, running in a static mode, following separation of Sr and Nd using conventional ion-exchange procedures as reported in Avanzinelli et al. (2005). Measured $^{87}Sr/^{86}Sr$ ratios were normalized to $^{88}Sr/^{86}Sr = 8.375209$, $^{143}Nd/^{144}Nd$ ratios to $^{146}Nd/^{144}Nd = 0.7219$. During collection of isotopic data, replicate analyses of the Sr NIST SRM 987 ($SrCO_3$) isotopic standards gave an average $^{87}Sr/^{86}Sr$ value of 0.710251 ± 20 ($2\sigma_m$, $N = 100$) well in agreement with the reference value of Thirlwall (1991). The in-house Nd isotopic standard NdFi (Nd oxide) was used to test reproducibility. Data are reported in Supplementary Material Table S10.

One leucogranite sample from the Sette Fratelli Unit (Stage 2), which represents the last magmatic episode in the Sarràbus pluton, post-dating the studied episyenites, was selected for $^{40}Ar/^{39}Ar$ dating. Amphibole crystals were separated by handpicking and then analysed at the Argon Geochronology Laboratory, Oregon State University (OSU), USA. The sample and sanidine flux monitors (Fish Canyon Tuff—FCT-2-NM, 28.201 ± 0.023 Ma, 1σ; Kuiper et al., 2008) were irradiated for 6 h at 1 MW power lux at OSU TRIGA reactor. Isotopic measurements were conducted using a multi-collector ARGUS-VI mass spectrometer and according to the method reported by Cano et al. (2024). Data reduction was performed with Ar-Ar Calc 2.7.0 software (Koppers, 2002). Data are in Supplementary Material Table S11.

Finally, mineral abbreviations used throughout this paper are according to IMA recommendations (Warr, 2021) as follows: Di (diopside), Hd (hedenbergite), Aeg-Aug (aegirine-augite), Hst (hastingsite), Act (actinolite), Adr (andradite), Bt (dark mica), Ab (albite), An (anorthite), Kfs (K-feldspar), Qz (quartz), Mag (magnetite) and Ttn (titanite).

4. Petrographical and mineralogical features

4.1. Petrographical features of granodiorites

Petrographical features of granodiorites are reported in Secchi et al. (2022). According to these Authors, granodiorites represent a sequence of magmatic pulses constituting the Cala Regina group which include septa of mafic rocks of gabbroic composition.

Granodiorites show commonly equigranular hypidiomorphic texture and are composed by euhedral crystal of zoned plagioclase laths, Fe-biotite and Fe-hornblende, followed by anhedral grains of quartz and K-feldspar. Accessory phases are ilmenite (on dark mica and quartz), zircon and apatite (on dark mica), euhedral allanite and rare titanite. Locally, (Capo Carbonara) titanite occurs as continuous edges along primary dark mica and ilmenite. Main observed differences between the different magmatic pulses of granodiorite are the southward increase of (a) size and incidence of microgranular dark enclaves mainly of quartz-gabbroic composition; (b) colour index from 14% to 20%; (c) occurrence of primary Fe-hornblende (1%–4% Vol.; Mg# 0.40–0.36 calculated as $Mg^{2+}/(Mg^{2+}+Fe^{2+}_{tot})$ mol.); plagioclase feldspar shows commonly discontinuous zoning ($An_{45–41}$) with calcic relic cores ($An_{63–39}$) (D'Angelo, 1998; Franciosi et al., 2019).

4.2. Episyenite textures

As commonly observed in intrusive complexes suffering metasomatic processes, the episyenites from Sàrrabus pluton show a wide range of compositional and textural characters (Fig. 3). However, some of them are ubiquitous as the occurrence of albititic plagioclase as a major constituent, a skarn-like mineral assemblage represented by diopsidic clinopyroxene and andraditic garnet as well as titanite and magnetite as main accessory phase (Fig. 3). In addition, quartz is only locally observed in aplo-pegmatitic veins from inhomogeneous bodies (Fig. 3l).

Spotted rocks show commonly coarse-grained heterogranular rock-textures (Fig. 3a, b, c, d). In the homogeneous outcrops, they schematically consist of a variably albitized plagioclase and anhedral to subhedral K-feldspar with interstitial domains filled by mafic minerals (up to 22% vol.) similarly to those described by Pérez-Soba and Villaseca (2019) for la Pedriza intrusion in the central Iberian Belt. Mafic minerals occur as aggregates of anhedral colorless to pale green diopside, partially or totally replaced by hastingsitic amphibole, which give rise to a spotted "leopard skin-like" macroscopic aspect as defined by Pirinu et al. (1996). In spotted rocks, large albite crystals replace primary patchy zoned plagioclase feldspar derived from the granodiorite protolith and, in addition, albite + dark mica occur as micro granoblastic aggregates along intergranular to sub-granular boundaries. Remarkably, spotted rock of inhomogeneous bodies at the top of granodioritic intrusions show in addition the following main textures: chessboard albite replacing K-feldspar is commonly observed accompanied by a large incidence of amphibole (replaced in turn by dark mica) on original

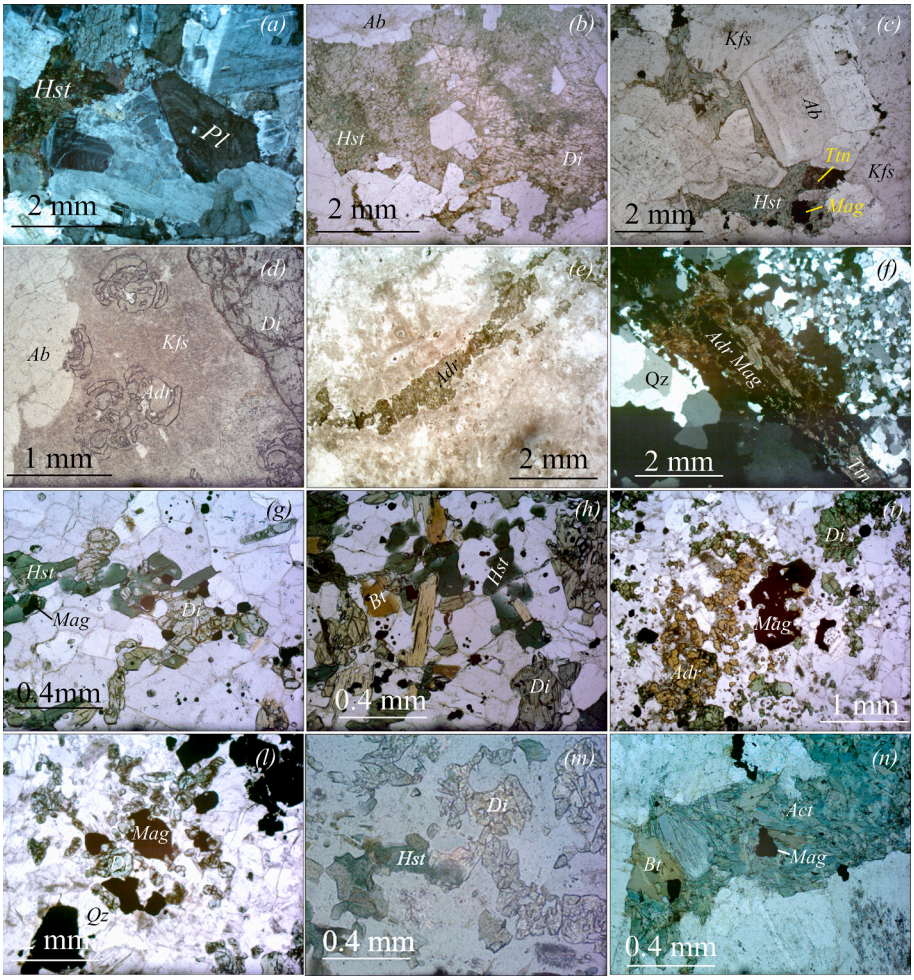

Fig. 3. Petrographic characters of episyenites from Sàrrabus pluton (SE Sardinia, Italy): (*a*) Textural aspects of episyenitic spotted rocks. Interstitial mafic mineral aggregates with respect to relics of euhedral patchy zoned plagioclase feldspar of andesine composition (Pl; Sedda sa Zarra). Crossed nicols. Sample R1; (*b*) Wide diffusion of anhedral colorless diopsidic clinopyroxene (Di) replaced by hastingsitic amphibole (Hst) on episyenitic spotted rocks (Sedda sa Zarra). Plane polarized light. Sample S6–9; (*c*) Automorphic texture of spotted episyenite with large euhedral albite crystals and interstitial aggregates of pale- green hastingsite amphibole (Hst) associated to magnetite (Mag) after completely replaced, originary diopside (Di) (Marroccu). Plane polarized light. Sample SSP14A; (*d*) Skeletal grains of andraditic garnet (Adr) in anhedral K-feldspar (Kfs) from albititic leucocratic bands (Sedda sa Zarra). Plane polarized light. Sample Sedda2; (*e*) Trains of micro-granular andraditic garnet in albitite aplitic veins (Sedda sa Zarra). Plane polarized light. Sample PEGM-SEDDAS; (*f*) Wide diffusion of andraditic garnet, titanite (Ttn) and magnetite (Mag) in albititic pegmatites (Sedda sa Zarra). Crossed nicols. Sample SEDDAS 6–9; (*g*) Dark-green amphibole after sub-euhedral clinopyroxene in albitized dark enclave (Campu Longu). Plane polarized light, sample SSP46; (*h*) Wide diffusions zones of dark mica (Bt) in previous sample. S.P. Plane polarized light, sample SSP46; (*i*) Wide diffusion of reddish sub-euhedral andraditic garnet after pale green clinopyroxene in episyenite (Campu Longu, q173). Plane polarized light, sample, SSP52; (*l*) magnetite/pale green clinopyroxene relationships in quartz-bearing episyenite vein (Cuccureddus). Plane polarized light, sample SSP44. (*m*) Textural relationships between sub- euhedral colorless diopsidic clinopyroxene and dark-green amphibole in dark enclave (Nuraghe s'Arridellaxiu). Plane polarized light. Sample ASP14; (*n*) Wide distribution of interstitial amphibole aggregates after originary clinopyroxene in episyenites (Sedda sa Zarra). Plane polarized light. Sample SSP14A. (For interpretation of the references to colour in this figure legend, the reader is referred to the web version of this article.)

clinopyroxene and magnetite; skeletal andraditic garnet precedes the K-feldspar crystallization (Fig. 3d); local zones of mortar quartz are observed; lastly, occurrence of dark inclusions of spotted rocks showing similar textural features of hosted rocks (Fig. 3m).

In the composite bodies, spotted rocks grade inhomogeneously to whitish and leucocratic rocks, and to bands characterized by micro-perthitic K-feldspar commonly replaced by chessboard albite, by abundant magnetite and andraditic garnet. Conversely, the secondary amphibole after clinopyroxene is lacking. Magnetite is observed as an intergranular phase or along sub-granular boundaries of deformed K-feldspar crystals.

In the composite outcrop of Campu Longu, medium-grained leucocratic rocks represent the prevailing rock-type. Overall, they represent deeply metasomatized rocks showing xenomorphic or granoblastic textures in which andraditic garnet is more frequent and developed, often occurring as continuous coronas on green clinopyroxene (Fig. 3i).

Decimetric aplo-pegmatitic veins are observed in composite bodies and range in composition from quartz-bearing episyenites to true albitites (Fig. 3l). Quartz-bearing varieties are essentially composed of K-feldspar micro-perthite and quartz showing mortar textures in pegmatites (up to 10% in volume) and minor amounts of amphibole replaced by small biotite flakes (Fig. 3h). Remarkably, andraditic garnet occurring as small intergranular grains represents the main accessory phase accompanied by well-developed apatite, allanite and titanite. In the aplitic veins from Campu Longu outcrop, quartz and K-feldspar coexist with green clinopyroxene and abundant large magnetite grains (Fig. 3l). Finally, true albitites, locally observed in the uppermost part of bodies (Sedda sa Zarra), consist essentially of an inequigranular aggregate of albite with apatite and titanite as accessory phases.

4.3. Feldspars

Representative compositions of feldspars are reported in Supplementary Table S1. Overall, originary plagioclase and K-feldspar framework from granodiorites is documented in spotted rocks, decreasing from homogeneous to composite bodies. Primary plagioclase exhibits typical patchy zoned textures documented in granodiorites, ranges in composition from An_{40} to An_{25} and is progressively replaced from albite pseudomorphs. Compositionally, albite in different textural contexts (i.e. euhedral, chessboard or microgranules; Table S1) ranges from An_1 to An_8. Conversely, the Fe_2O_3 contents increase in the range of 0.01 to 0.27 wt% and reach more than 3 wt% in microgranular grains from Campu Longu outcrop. Locally, it suffered some degree of deformation, as suggested by curved or faulted twining lamellae (Pirinu et al., 1996). In small homogeneous bodies, coarse plagioclase grains are replaced by continuous microgranular aggregates of albite grains either along crystal rims or fractures. Incidence and textures of K-feldspar change considerably in the observed samples; originary Carlsbad twinned perthitic orthoclase occurring as anhedral grains is progressively replaced in composite bodies by microcline microperthite with a tartan twinning which prevail in leucocratic bands and veins. Some K-feldspar grains are partially to completely replaced by chess board albite or pervasively replaced by microgranular aggregates or by single crystal, albite-twinned skeletal grain.

In Campu Longu body, feldspar framework is made up of inequigranular allotriomorphic aggregate of often more developed microcline perthite prevailing on albite crystals which show in addition fractures filled by granular albite (Brotzu et al., 1978). No relic plagioclase from originary granodiorite was observed.

4.4. Clinopyroxene

Representative compositions are reported in Supplementary Table S2, and classified according to IMA's constraints (Morimoto, 1989). Clinopyroxene represents ubiquitous mafic mineral occurring in various amounts in every rock-type decreasing in modal content from spotted rocks to leucocratic veins. In spotted rocks, it commonly occurs as large pale anhedral crystals or as greenish clear sub-euhedral; in the episyenite and leucocratic veins from Campu Longu outcrop it forms drop-like clusters (Fig. 3g). Overall, clinopyroxene can be classified as diopside (Wo > 45%) close to the boundary with hedenbergite and approaches aegirine-augite composition in episyenite rocks from Campu Longu (Fig. 4). Remarkably, chemical compositions from spotted rocks and Campu Longu episyenites, show distinctive trends in plots constructed with $Mg_{\#}$ (Fig. 4). Clinopyroxene in spotted rocks show commonly low Al^{IV} and Na contents (0.005–0.028 a.p.f.u.) and Fe^{3+} (0.070–0.040 a.p.f.u.), while Ti drops to zero (< 0.003 a.p.f.u). Conversely, clinopyroxene from Campu Longu, exhibits higher Ti, Al^{IV} and Na contents with a more marked inverse correlation with $Mg_{\#}$; in this outcrop, higher Na values are recorded for clinopyroxene from episyenite samples close to the gabbroic rocks.

Lastly, clinopyroxenes from leucocratic veins and metasomatized dark enclaves from different outcrops, display comparable values plotting at the end of described trend of spotted rocks (Fig. 4).

4.5. Amphibole

In studied metasomatized rocks, amphibole occurs mainly after clinopyroxene and appears positively correlated with modal contents of magnetite. In spotted rocks, amphibole occurs as pale green to green crystals overgrown on clinopyroxene or interstitial granoblastic aggregates, respectively, documenting an increasing replacement process. In coarse recrystallized rocks from Campu Longu, as well as in dark enclaves related to spotted rocks, it is more diffuse and occurs as microgranular subhedral dark green crystals often replaced in turn by brownish dark mica. Fibrous radial aggregates on quartz are locally observed in pegmatitic veins of composite bodies.

Representative compositions of amphiboles from metasomatized rocks are included in Supplementary Table S3. According to IMA's constraints (Hawthorne et al., 2012), in these rocks, amphiboles range in composition from Mg-hastingsite to hastingsite with respect to gabbroic and granodiorite host rocks which are characterized by Mg-hornblende and Fe-hornblende, respectively. As observed for clinopyroxene composition, amphiboles from Campu Longu bodies reveal compositional differences with respect to spotted rocks and related composite bodies in terms of higher Na and Al^{VI} and, conversely, lower Mn contents.

Overall, all analysed amphiboles show positive Al_{Tot} - Na correlation (Fig. 5a) and a negative Ca-Na correlation (Fig. 5b) which, on account of positive Na-Fe^{3+} (Fig. 5c) correlations.

Lastly, a progressive continuous trend may be observed when comparing episyenites with Cala Regina host rocks (Fig. 5b; c).

4.6. Garnet

Garnet occurs in more albitized rocks lacking in spotted varieties and, according to Meagher (1982) and Cuney et al. (2012), shows textural and chemical characters typical of metasomatic processes. It occurs mainly as aggregates of subhedral grains associated with titanite and magnetite and appears to be preceded by clinopyroxene crystallization. In rocks from Campu Longu, it occurs mostly as reddish aggregates, locally overgrowing the pale-yellow crystals. Representative

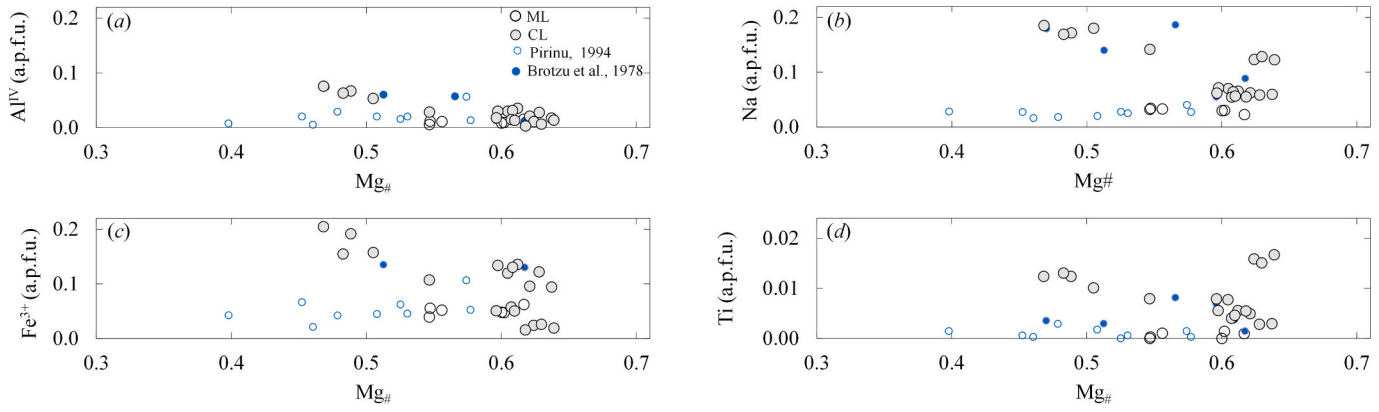

Fig. 4. Compositional variations of clinopyroxene from episyenitic rocks of Sàrrabus pluton. SZ and CL refer to clinopyroxene from Sedda sa Zarra and Campulongu outcrops, respectively. For comparison are reported data after Pirinu (1994) and after Brotzu et al. (1978). Note the common different trend followed by clinopyroxene from Campulongu with respect to those observed for Sedda sa Zarra Campu Longu area.

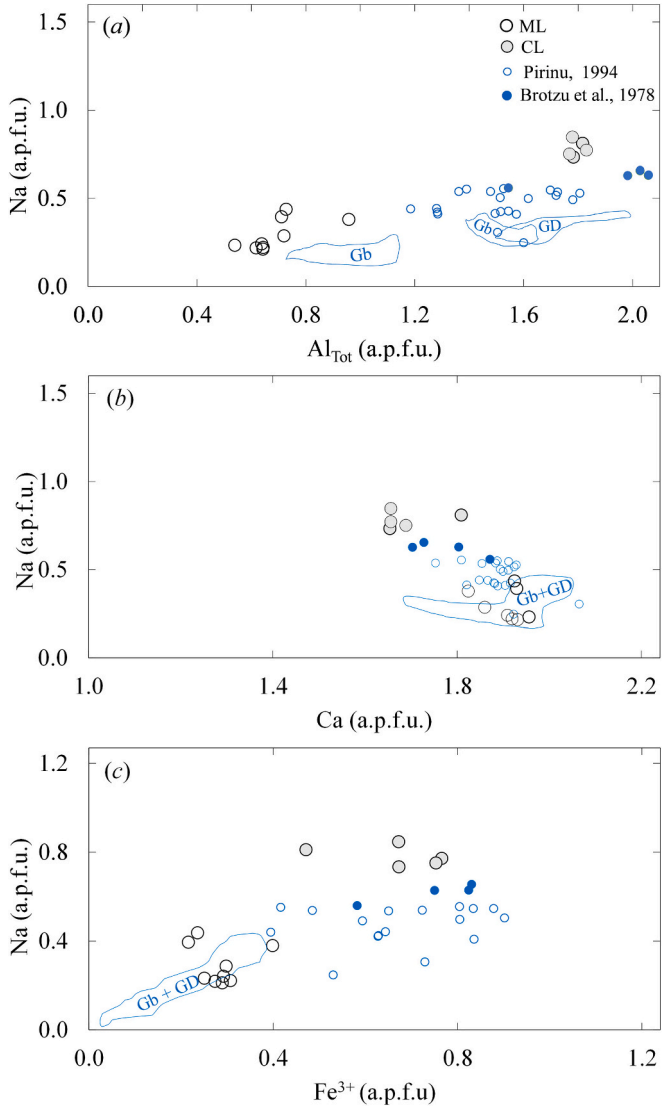

Fig. 5. Compositional variations of amphiboles from episyenitic rocks of Sàrrabus pluton. SZ and CL refer to clinopyroxene from Sedda sa Zarra and Campulongu outcrops, respectively. For comparison are reported data after Pirinu (1994) and after Brotzu et al. (1978). Note the progressive Na enrichment trends of amphibole from Sedda sa Zarra with respect to those observed for Campulongu. Gb and GD refer to amphiboles from gabbroic and granodiorite host rock, respectively, belonging to Cala Regina group, after D'Angelo (1998), Poli and Tommasini (1999), Conte et al. (2017) and Franciosi et al. (2019).

chemical analyses of garnets are reported in Table S4. According to IMA's recommendations (Grew et al., 2013) all analysed garnets may be generally classified as andradite and, on the ground of a systematic Fe^{3+} > Ti a.p.f.u., better defined as melanite as expected in metasomatic processes (Russell et al., 1999).

Overall, all the analysed crystals show rather homogeneous composition, low Fe^{2+} content and a quite low solid solution between andradite and grossular and members with minor proportions of schorlomite and morimotoite-Mg with only insignificant incidence of pyrope and almandine. However, a slight spessartine enrichment is observed for reddish garnet from Campu Longu.

4.7. Accessory phases

Representative compositions of magnetite, which is a ubiquitous, and main accessory phases are reported in Supplementary Table S5. Magnetite is usually euhedral, as isolated sub-millimetric grains or in aggregates. Commonly it appears closely associated with amphibole pseudoparamorphs aggregates in spotted rocks, while at Campu Longu it is observed as inclusions in dark green amphibole or, locally, in clinopyroxene (Fig. 3i), frequently associated with titanite. Magnetite plots on the magnetite-hematite tie line close to the ideal composition of magnetite, with minor and variable contents of TiO_2, MnO, MgO, SiO_2, and Al_2O_3 (Supplementary Table S5).

Titanite (Table S6) represents a widespread accessory mineral. It lacks in amphibole-free spotted rocks. It occurs commonly as crystals associated with magnetite in two textural types: (1) anhedral crystals associated with amphibole in spotted rocks or (2) subhedral crystals associated to andraditic garnet in pegmatites. With respect to analysed titanite reported in Pérez-Soba and Villaseca (2019) for La Pedriza albitites, Sàrrabus titanites show a more pronounced Al content in the range of 0.053–0.080 a.p.f.u.

5. Whole rock analyses

5.1. Major and trace elements

Major and trace element compositions of Sàrrabus episyenites are given in Table S8 to complete the published analytical picture available in Brotzu et al. (1978) and Pirinu et al. (1996).

In the TAS (Total Alkali versus Silica) classification diagram (Fig. 6), episyenites plot in alkali field and show a broad compositional trend with a roughly SiO_2 – Na_2O + K_2O positive correlation. The episyenites display a broad compositional range in Na_2O, which shows roughly negative correlations with K_2O (Fig. 7a). The K_2O and Rb contents show a positive correlation (Fig. 7b); lower values are observed for samples characterized by chessboard albite. Strontium and Ti are positively correlated with CaO (Fig. 7c; d).

The chondrite-normalized REE (Fig. 8a) and PM-normalized trace

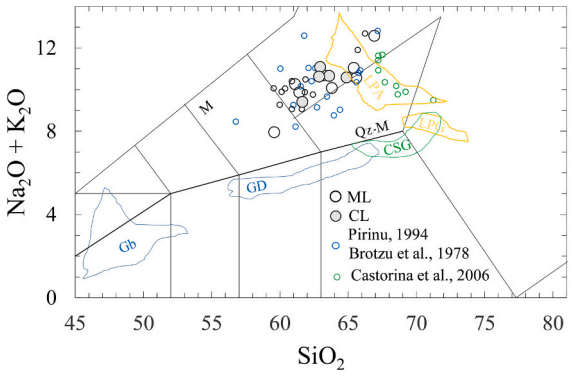

Fig. 6. TAS classification diagram according to Middlemost (1994) constraints for episyenitic rocks from late-Variscan Sàrrabus pluton. ML and CL refer to episyenites from Sàrrabus pluton reported in Table S.1 (ML from Sedda sa Zarra, Nuraghe s'Arriudellaxiu, Cuccuru Ella and Marroccu outcrops; CL after Campulongu and Cuccureddus outcrops). ML includes three samples from Rizzo (1994) analysed with the same technique ICP-MS. For comparison are reported data from XRF after Pirinu (1994) (Sedda sa Zarra, Cuccuru Ella and N.ghe s'Arridellaxiu outcrops) and Brotzu et al. (1978) (Campu Longu and Cuccureddus outcrops); Castorina et al. (2006) refer to albitized rocks from central Sardinia. Gb and GD refer to gabbroic and granodioritic rocks from Cala Regina group of Sàrrabus pluton (data after Poli and Tommasini, 1999; Franciosi et al., 2019; Secchi et al., 2022). LPA and LPG yellow fields refer to albitized rocks and their host granites from La Pedriza pluton (central Spanish system; data after Perez-Soba and Villaseca, 2019), respectively. CSG field refer to unaltered granitoids from central Sardinia (data after Castorina et al., 2006). M, Qz-M and Sy refer to monzonite, Qz-monzonite and syenite fields, respectively. See purple-colored numbers in the geological map attached to the paper (Fig. 1) for outcrop localizations. (For interpretation of the references to colour in this figure legend, the reader is referred to the web version of this article.)

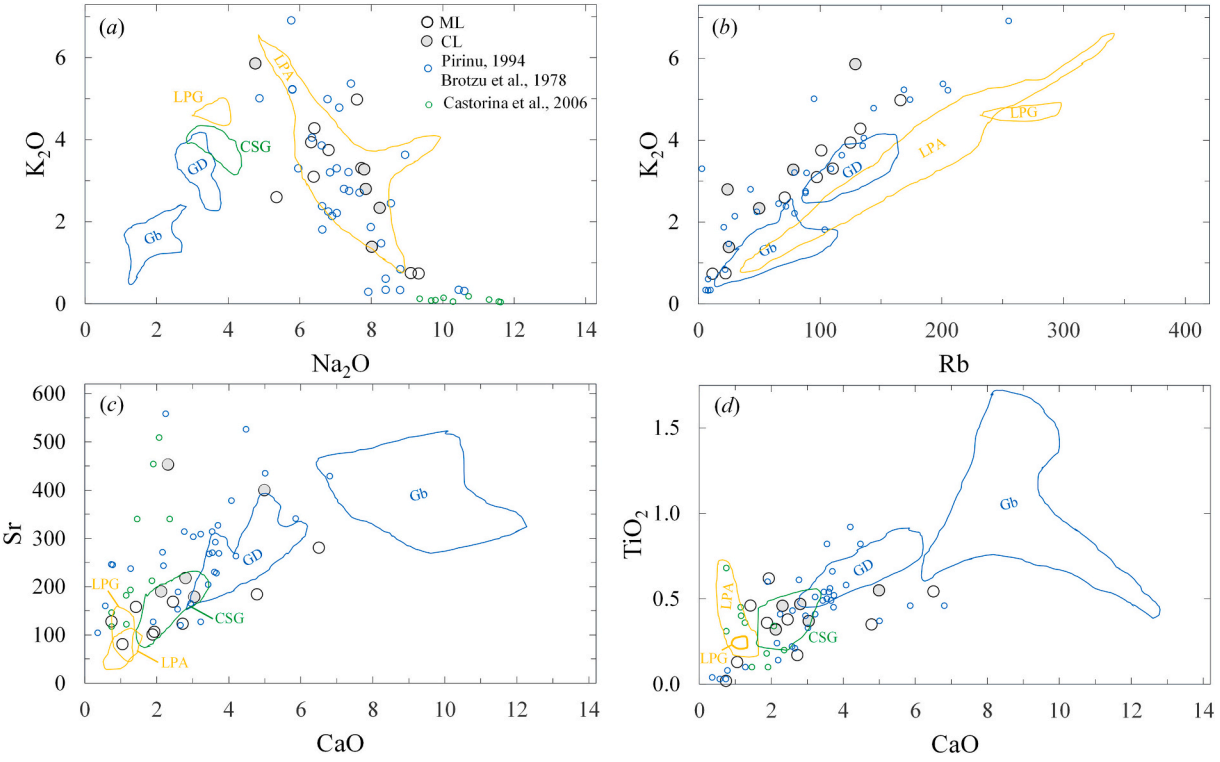

Fig. 7. Whole-rock chemical variations of selected trace elements for the episyenites from Sàrrabus pluton. ML and CL refer to episyenites from Sàrrabus pluton reported in Table S.1 (ML from Sedda sa Zarra, Nuraghe s'Arriudellaxiu, Cuccuru Ella and Marroccu outcrops; CL after Campulongu and Cuccureddus outcrops). For comparison are reported data after Pirinu (1994) (Sedda sa Zarra, Cuccuru Ella and N.ghe s'Arridellaxiu outcrops) and Brotzu et al. (1978) (Campu Longu and Cuccureddus outcrops); Castorina et al. (2006) refer to albitized rocks from central Sardinia. Gb and GD refer to gabbroic and granodioritic rocks from Cala Regina group of Sàrrabus pluton (data after Poli and Tommasini, 1999; Franciosi et al., 2019; Secchi et al., 2022). LPA and LPG yellow fields refer to albitized rocks and their host granites from La Pedriza pluton (central Spanish system; data after Perez-Soba and Villaseca, 2019), respectively. CSG field refer to unaltered granitoids from central Sardinia (data after Castorina et al., 2006). (For interpretation of the references to colour in this figure legend, the reader is referred to the web version of this article.)

elements patterns (Fig. 8b) are quite similar to those observed for host granodiorites, although of a slight LREE general decrease and, on the contrary, a HREE enrichment observed for garnet-bearing pegmatitic pods from Sedda sa Zarra (Fig. 8a).

5.2. Isotope data

To constrain the age of Sàrrabus episyenites, titanite, which represents a ubiquitous U-bearing metasomatic mineral phase in studied samples, has been chosen to provide data to compare with geological and published radiometric ages. Titanite in the analysed sample is mainly associated with magnetite and andraditic garnet. It commonly shows homogeneous composition in backscattered images. Few crystals show a faint, thin (10 μm) patchy zoning and, more rarely, oscillatory (Fig. 9a-d). U/Pb isotopic LA-ICP-MS analyses of a representative sample of pegmatitic vein from Sedda sa Zarra outcrop (Table S9), provide an isochron age of 279 + 15/-22 Ma (n = 24; MSWD = 1.9; Fig. 9e). Remarkably, the 279 Ma value is indistinguishable, within the correlated error (+15/-22), from the 286 ± 15 Ma (MSWD = 0.97; *fit* probability = 44%) data obtained by Secchi et al. (2021) by U-Pb, LA-ICP-MS zircons analyses from hosting biotite and hornblende granodiorite of Capo Carbonara, close to the Campu Longu outcrop (Fig. 1).

In addition, to better constrain the igneous activity of the Sàrrabus pluton and indirectly, the time of the metasomatic event, we date the granite belonging to the Sette Fratelli Unit (stage 2) which, according to Secchi et al. (2021) represents the last intrusive episode of Sàrrabus pluton. According to Conte et al. (2017), amphibole in these rocks is an euhedral early crystallizing phase, optically and chemically homogeneous. The multi-fragment step heat analysis for $^{40}Ar/^{39}Ar$ dating of amphibole crystals yielded a plateau age of 286 ± 1 Ma (2σ error; 89% of ^{39}Ar released, n = 16, MSWD = 8.97, K/Ca = 0.122), identical to that obtained from normal isochron (Supplementary Material Table S11).

Episyenites from Sàrrabus pluton provide $^{87}Sr/^{86}Sr$ ratios in the range of 0.710921 ± 0.000006 and 0.725774 ± 0.000006 and $^{143}Nd/^{144}Nd$ ratios between 0.512127 ± 0.000004 and 0.512361 ± 0.000011 (2σ error; Supplementary Table S10).

In the Rb-Sr and Nd-Sm isochron plot (Fig. 10a, b), only the episyenitic rocks and hosting granodiorites with microgranular hornblende quartz-gabbroic rocks cluster on a 286 Ma reference line (according to published Pb/Pb chronological data: Secchi et al., 2021). Thus, we recalculated the Sr and Nd isotopic ratios at 286 Ma as episyenites formation age.

Initial $^{87}Sr/^{86}Sr$ ratios are between 0.709226 and 0.711401 and $^{143}Nd/^{144}Nd$ ratios are between 0.511921 and 0.511949 with εNd_{286} between -6.84 and -6.29. Isotopic initial ratios do not show correlations with SiO_2, P_2O_5/K_2O and elemental concentrations. In the $^{87}Sr/^{86}Sr_{286}$ vs εNd_{286} diagram (Fig. 11), epysienites plot from the granodiorite field toward the peraluminous granites of Stage 1 from Secchi et al. (2022) showing a common more radiogenic Sr isotopic composition with respect to the first intrusives.

6. Discussion

6.1. Classification aspects of episyenite

The classification of studied rocks and the attribution to a specific family of metasomatized rocks is difficult. According to the International Union of Geological Sciences (IUGS) recommendations for

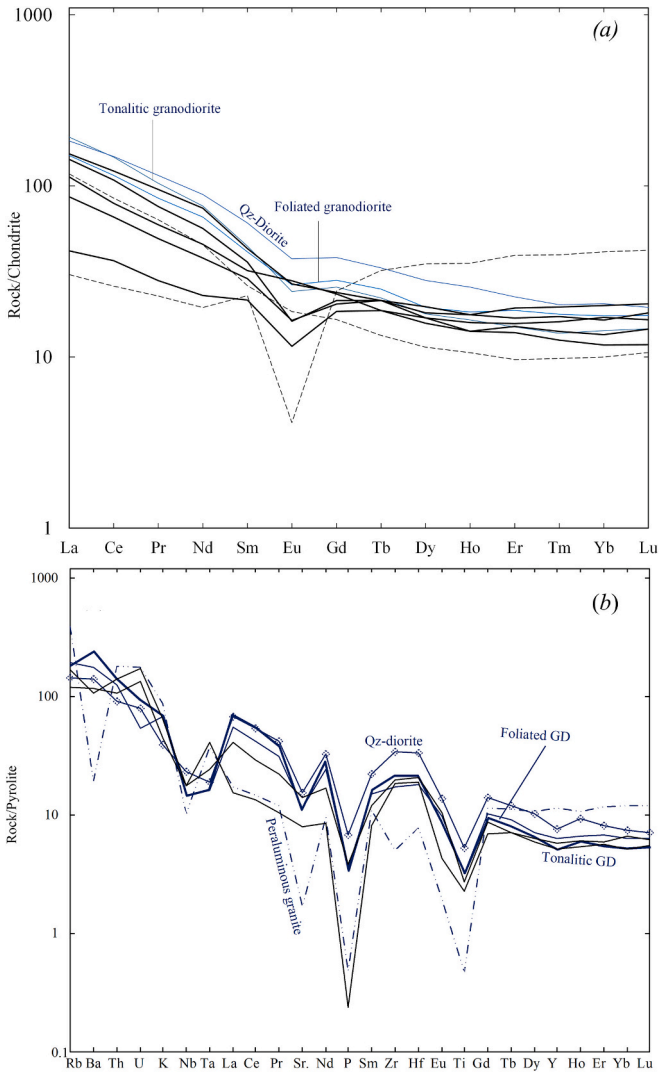

Fig. 8. Whole-rock chondrite-normalized REE patterns (a) and Spyder diagram (b) for Sàrrabus episyenites (black-colored) and host granodiorites (light blue colored; data after Secchi et al., 2022). Dashed black lines refer to pegmatitic pods and aplitic sub-vertical quartz-bearing veins associated with episyenites. Normalizing values to chondrite-I after Sun and McDonough (1989) and to primitive mantle pyrolite model of Mc Donough and Sun (1995). (For interpretation of the references to colour in this figure legend, the reader is referred to the web version of this article.)

nomenclature of shear zone-related metasomatic rock-types (Zharikov et al., 2007), studied rocks should be classified as albitites. However, they are commonly characterized by a "skarn-like" mafic mineralogy, instead of the expected riebeckite and/or aegirine assemblage. Overall, their general features are close to episyenites (Cuney et al., 2012; Suikkanen and Rämö, 2019), while revealing several affinities with sodic fenites (Elliott et al., 2018) as observed for coeval metasomatic varieties from La Pedriza in central Iberian belt (Pérez-Soba and Villaseca, 2019). Moreover, the Authors prefer the general term of episyenites addressing the term of albitite to hololeucocratic vein varieties almost composed by albite.

6.2. Geological and petrographic constraints

Field relationships constrain the source of metasomatic fluids to the hosting granodiorites. Indeed, the epsyenites are confined to a narrow *syn*-plutonic shear zone (Fig. 1c) which drives the pluton growth as a result of extensional regime. No similar rocks have been found in the intrusives related to Stage 2 or in basement rocks. The sharp contacts with host granodiorite (Fig. 2c; d) is further evidence of metasomatism occurring during emplacement of granodioritic magma pulses. In addition, episyenites pre-date the granitic intrusions of the Sàrrabus pluton and, conversely, are crosscutted by mafic dikes (Pirinu et al., 1996), related to the latest magmatic events of Stage 2 (Secchi et al., 2022).

Alkali metasomatized spotted rocks locally preserve original textural and mineralogical features of granodiorites (i.e. patchy zoned plagioclase feldspar; Fig. 6a) suggesting roughly isovolumetric metasomatic alteration.

Conversely, deeply metasomatized rock-types show a xenomorphic or granoblastic texture unrelated to the original rock, and contain in addition andraditic garnet coexisting with a more Na-rich clinopyroxene close to aegirine-augite compositions (Table S2). Overall, a Na increase is observed in both clinopyroxenes and amphiboles reflecting the double substitution $Ca^{2+} + Fe^{2+} = Na^{+} + Fe^{3+}$ according to Shearer and Larsen (1994).

The compositional differences between the host granodiorites and episyenites are illustrated in the shift from subalkaline to alkaline field in the TAS diagram (Fig. 6), where episyenite compositions essentially mimic those of alkaline magmatic rocks in response to chemical variation of hosting granodiorites, as well as by a general decrease in Rb and Sr (Fig. 7). Sàrrabus episyenites show a different composition with respect to Late-Variscan high temperature albitized rocks from La Pedriza pluton (Pérez-Soba and Villaseca, 2019), which plot at the end of hosting peraluminous leucogranites in the TAS diagram (Fig. 6). In addition, as expected for different protoliths, La Pedriza albitized rocks show lower values of Sr - substantially indistinguishable from hosting leucogranites - with respect to studied rocks (Fig. 7).

Chemical variations during alteration of Sàrrabus granodiorites, can be shown in the *Q–P* multicationic diagram (Fig. 12) in which the analysed episyenites document a broad Na-stage with roughly constant *Q* which correspond to crystallization of albite, and/or diopside and Ca-amphiboles as interstitial phases (arrow 2), leading to the formation of episyenites. Curiously, no evidence of desilication trend due to quartz dissolution (arrow 1 in Fig. 12), a common feature documented in other districts (e.g. central Ukraine, Cuney et al., 2012; Japan, Nishimoto et al., 2014; Finland, Suikkanen and Rämö, 2019), is observed.

Overall, the observed mineral assemblage of episyenite provides useful indications of *T*, fO_2 and water activity during crystallization. Indeed, the common occurrence of a mafic assemblage with early clinopyroxene and amphibole point to high-*T* processes. In addition, magnetite as only opaque phase, coupled to lack of wollastonite are evidence in favor of high fO_2, further confirmed by the Fe^{3+} enrichment trend of amphibole from gabbroic to hosting granodioritic rocks and episyenites (Fig. 5c); water activity increase is evidenced by the clinopyroxene - amphibole relationships.

The Campu Longu mineral assemblages display distinct characters. Composition of clinopyroxene and amphibole records a more pronounced Na enrichment in episyenitic rocks close to gabbroic masses, thus suggesting a possible relationship between the fluid source and mafic components.

6.3. Physico-chemical estimates

Physico-chemical estimates for episyenitic rocks are reported in Table S7. The use of Al-*in* titanite, according to Erdmann et al. (2019) calibration, provides value of 1.9 ± 0.02 kbar, which is indistinguishable with those observed for tonalite and hornblende gabbroic varieties when using the Al-*in* hornblende calibration by Ridolfi (2021). Estimates for latest Sàrrabus granites show definitely lower *P* values, clustered around 1 kbar on the basis of fluid inclusions (Frezzotti, 1992).

Thermometric constraints for episyenites may be offered by the recent Ti-*in* amphibole calibration proposed by Liao et al. (2021) as well as Zr-*in* titanite which provide values clustered at 700 °C when using the lower Zr contents which represent equilibrium zones according to

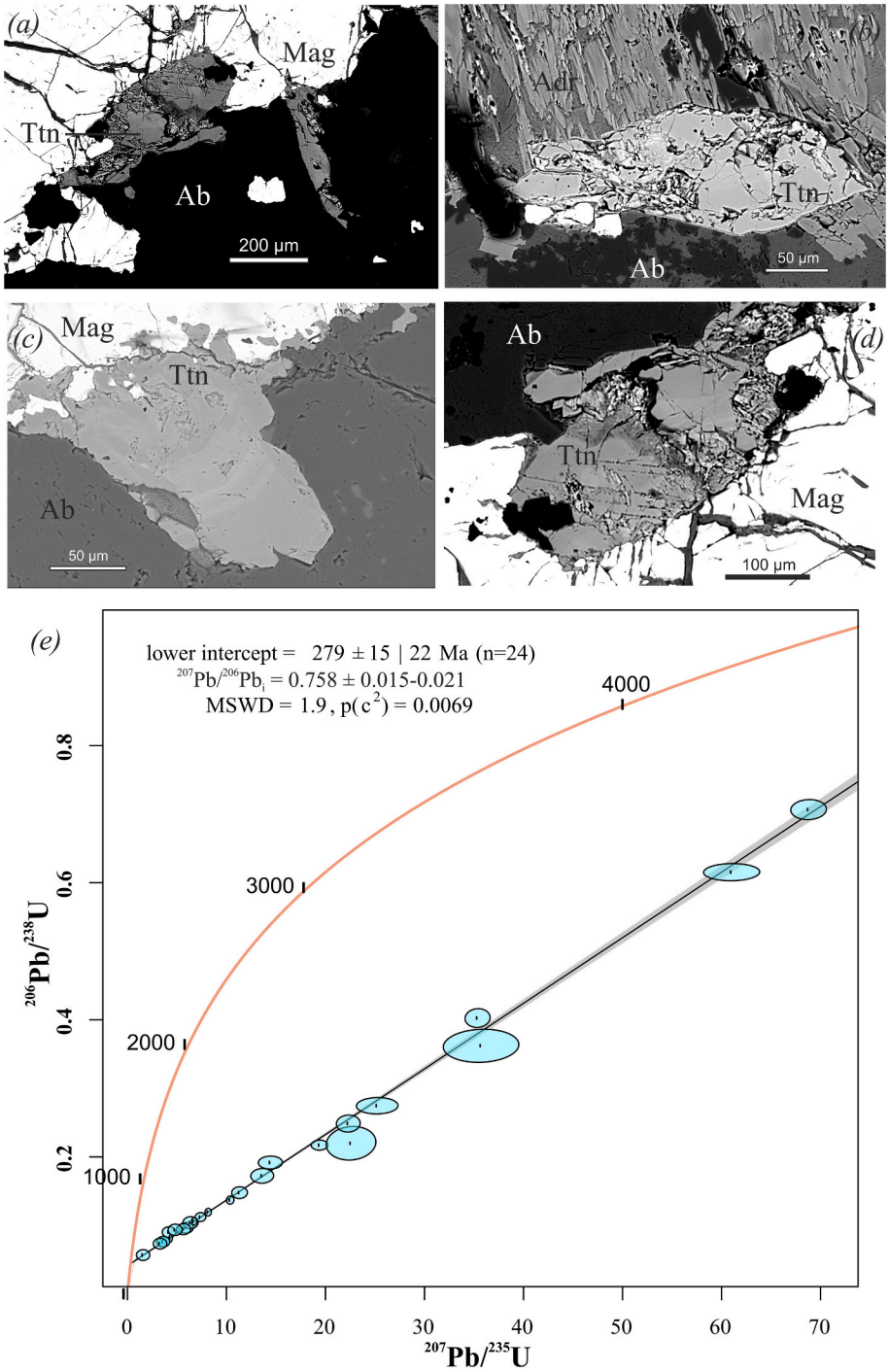

Fig. 9. (*a-d*) BSE images of titanite crystals in the PEG M SEDDAS sample from Sedda sa Zarra outcrop (❶ in Fig. 1), often associated with magnetite (Mag), albite (Ab). Titanite is mainly homogeneous in BSE (e.g. *a-b*), with only few crystals showing a very faint zoning (i.e. *c-d*); (*e*) U-Pb lower intercept age of PEG M SEDDAS sample on a Wetherill U-Pb concordia diagram constructed with 24 analysed points -via LA-ICP-MS- reported in Table S.9. MSWD = 1.9; pc^2 = 0.0069. Data point error bars and weighted age uncertainties are at the 2σ level.

Hayden et al. (2008) recommendations. Remarkably, these values are in good agreement with constraints imposed by phase relationships for the titanite-andradite-magnetite skarn system (Shoji, 1978; Wones, 1989). In addition, the obtained values are not far from *solidus* of host rocks. Indeed, hornblende gabbroic varieties provide *T* values (close to the *liquidus*) of about 800–820 °C when using the hornblende/plagioclase calibration of Holland and Blundy (1994) assuming a P = 2.0 kbar. Similar values of 780 °C are obtained for granodiorite samples from Torre de su Fenugu.

Microblastic and deformed albite, observed in several samples, suggests a lower *T* limit at about 450 °C according to the minimum temperatures required for ductile deformation of feldspars (Doi et al., 2009), as observed in other Na-metasomatic episyenites (Cuney et al., 2012) and in good agreement with data obtained for Zr-*in* quartz of pegmatitic varieties from Sedda sa Zarra.

Estimates of fO_2 according to the equation of Wones (1989) provide values between -18.5 to -14.8 (Table S7), between the NNO-HM buffers, in good agreement with the constraints provided by Shoji (1978) and

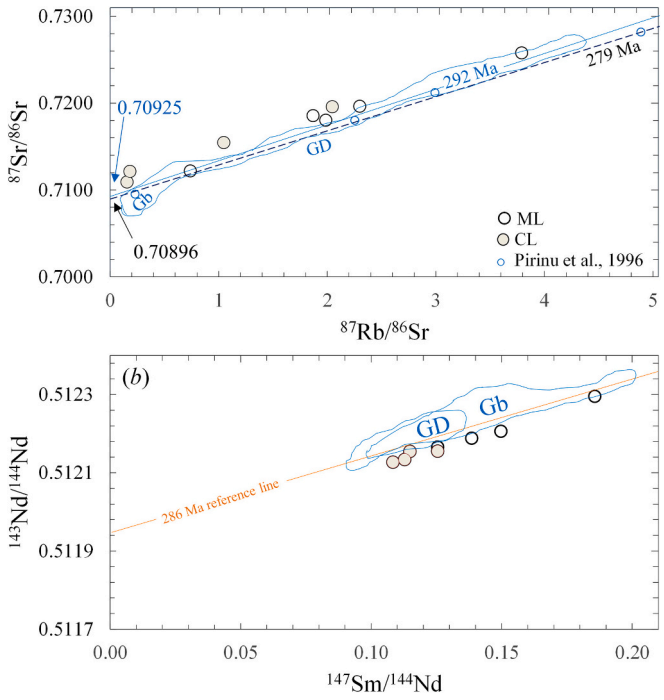

Fig. 10. Whole-rock Rb-Sr (*a*) and Nd-Sm (*b*) isochron plots showing behaviour between the evolution of episyenites and hosting granodiorites and associated gabbroic rocks from Cala Regina group of Sàrrabus pluton. Episyenites and hosting granodiorite samples cluster around the 286 Ma reference line constructed according to published Pb/Pb data on single zircons of hosting granodiorite from Capo Carbonara (Secchi et al., 2021). ML and CL refer to episyenites from Sàrrabus pluton reported in Table S.1 (ML from Sedda sa Zarra, Nuraghe s'Arriudellaxiu, Cuccuru Ella and Marroccu outcrops; CL after Campulongu and Cuccureddus outcrops). For comparison are reported data after Pirinu (1994) (Sedda sa Zarra, Cuccuru Ella and N.ghe s'Arridellaxiu outcrops). Gb and GD refer to gabbroic and granodioritic rocks from Cala Regina group of Sàrrabus pluton (data after Poli and Tommasini, 1999; Franciosi et al., 2019; Secchi et al., 2022).

Wones (1989) phase diagrams. Moreover, amphibole compositions satisfying the constraints requested by calibration of Ridolfi (2021) provide fO_2 values that fall in the same interval (Table S7).

Overall, physico-chemical estimates for episyenitic rocks will be compared with recalculated values obtained for gabbroic and granodiorite coeval host rocks from Cala Regina Group using data available in literature (Conte et al., 2017; D'Angelo, 1998; Franciosi et al., 2019; Poli and Tommasini, 1999).

6.4. *Age of the metasomatic event*

Several lines of evidence strongly support the pene-contemporaneity between granodiorite emplacement and metasomatic stages. This evidence is rather uncommon compared to similar metasomatic systems described in literature (Castorina et al., 2006; Cuney et al., 2012; Nishimoto et al., 2014; Pérez-Soba and Villaseca, 2019; Suikkanen and Rämö, 2019). In absence of regional post-magmatic significant thermal events, the above discussed calibrations constraining the *T* conditions at about 700 °C, confirm that the magmatic and metasomatic processes are substantially coeval. Geological constraints are confirmed by geochronology. Indeed, a U-Pb isochron obtained by in-situ titanite analyses, yielded a value of 279 +15/-22 Ma (Fig. 9e). Despite the high values of the correlated error (MSWD = 1.9; pc^2 = 0.0069) this age appears reliable, as it overlaps the age of 286 ± 2 Ma obtained by U/Pb on zircons collected in hosting granodiorites close to Campu Longu outcrop (Secchi et al., 2021). A Rb-Sr isochron calculated for spotted rocks provided an age of 294 ± 9 Ma (Pirinu et al., 1996).

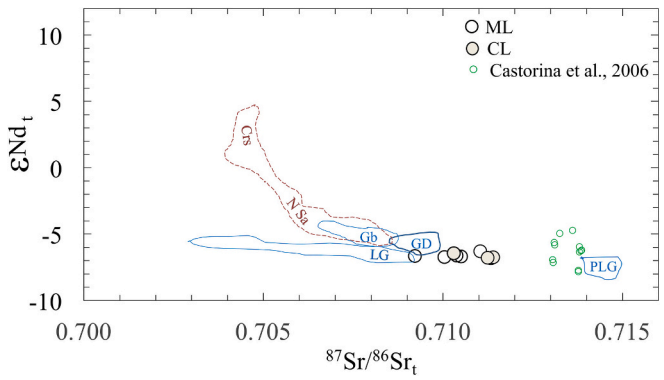

Fig. 11. $\varepsilon Nd_{(286)}$ vs. $^{87}Sr/^{86}Sr_{(286)}$ for episyenitic rocks from Sàrrabus pluton. Albitic rocks from Gocèano (central Sardinia) are reported for comparison (data after Castorina et al., 2006). ML and CL refer to episyenites from Sàrrabus pluton reported in Table S.1 (ML from Sedda sa Zarra, Nuraghe s'Arriudellaxiu, Cuccuru Ella and Marroccu outcrops; CL after Campulongu and Cuccureddus outcrops). For comparison are reported data after Pirinu (1994) (Sedda sa Zarra, Cuccuru Ella and N.ghe s'Arridellaxiu outcrops). Gb, GD, LG and PLG refer to gabbroic rocks, granodiorites metaluminous/subaluminous and peraluminous (Monte Maria Unit) leucogranites from Sàrrabus pluton, respectively (data after Poli and Tommasini, 1999, Franciosi et al., 2019 and Secchi et al., 2022). Dashed field refer to late-Variscan gabbroic rock-association from Corsica (Crs) and northern Sardinia (N Sa); data after Cocherie et al. (1994) (Corsica), Tommasini et al. (1995) (northern Sardinia) and Casini (northern Sardinia), personal communication.

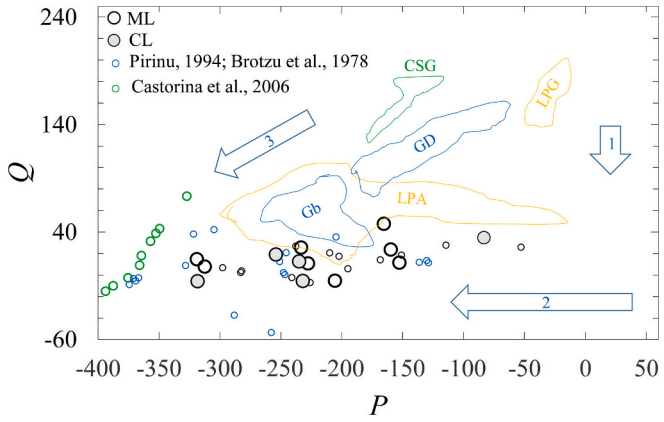

Fig. 12. feldspar (*P* parameter) – quartz (*Q* parameter) evolutive multi-cationic diagram for episyenitic rocks from Sàrrabus pluton. Arrows 1, 2 and 3 refer to desilicization, Na-metasomatism and Ca-metasomatism trajectories, respectively. $P = K - (Na + Ca)$ and $Q = Si/3 - (K + Na + 2Ca/3)$ according to Debon and Le Fort (1988). ML and CL refer to episyenites from Sàrrabus pluton reported in Table S.1 (ML from Sedda sa Zarra, Nuraghe s'Arriudellaxiu, Cuccuru Ella and Marroccu outcrops; CL after Campulongu and Cuccureddus outcrops). For comparison are reported data after Pirinu (1994) (Sedda sa Zarra, Cuccuru Ella and N.ghe s'Arridellaxiu outcrops) and Brotzu et al. (1978) (Campu Longu and Cuccureddus outcrops); Castorina et al. (2006) refer to albitized rocks from central Sardinia. Gb and GD refer to gabbroic and granodioritic rocks from Cala Regina group of Sàrrabus pluton (data after Poli and Tommasini, 1999; Franciosi et al., 2019; Secchi et al., 2022). LPA and LPG yellow fields refer to albitized rocks and their host granites from La Pedriza pluton (central Spanish system; data after Perez-Soba and Villaseca, 2019), respectively. CSG field refer to unaltered granitoids from central Sardinia (data after Castorina et al., 2006). (For interpretation of the references to colour in this figure legend, the reader is referred to the web version of this article.)

Lastly, the new $^{40}Ar/^{39}Ar$ plateau age of 286 ± 1 Ma obtained from amphibole from the leucogranite of the Sette Fratelli Unit (Supplementary Material Table S11) is indistinguishable from the 286 ± 2 Ma

age of Cala Regina Group intrusion.

Overall, collected ages and barometric estimates point to short-time emplacement of intrusions during a rapid uplift of the Sàrrabus region.

6.5. Isotopic constraints

The isotopic composition of episyenites plots at the end of general Sàrrabus trend between gabbroic/granodioritic rocks and crustal-derived peraluminous granites. Episyenites usually show a more radiogenic Sr composition and slightly lower $\varepsilon Nd_{(t)}$ values with respect to the hosting gabbroic and granodiorite rocks of Cala Regina Group (Fig. 11), confirming a direct relationship with the main magmatic event. Evidence in favor of this interpretation is also provided by overlapping $\delta^{18}O_{SMOW}$‰ values between granodiorites and episyenite rocks (Brotzu et al., 1983). In this frame, the isotopic composition of episyenites along the mafic-peraluminous trend (Fig. 11) indicate that the Na-metasomatism is related to the Stage 1 event (Secchi et al., 2022), before the onset of Stage 2, as confirmed by the overlapping ages between the episyenites and the hosting granodiorite. The shifting of Sr isotopic composition of the episyenites from the granodioritic field also indicates mobility of Sr during the metasomatic event in good agreement with mass balance calculation by isocon analysis (Fig. 13).

6.6. Metasomatic stages

Several stages of metasomatism are revealed by different mineral assemblages and supported by mineral chemistry. Early metasomatism of granodiorites is documented by precipitation of anhedral diopside and euhedral albite, followed by amphibole, and in turn by magnetite + andradite + titanite ± apatite. Late-stages of metasomatism display albite ± dark mica occurring as micro granoblastic aggregates along intergranular boundaries, and as chessboard albite replacing feldspars (Pirinu et al., 1996). Evidence in favor of local desilication and silica re-precipitation processes is the accidental presence of quartz, which is prevailingly found as mortar textures and in local veinlets. Overall, the variety of metasomatic stages producing some of the observed textural relationships may be schematized by classical reactions (Harlov et al., 2006) as follows:

$$9Hd + 2O_2 = Adr + Mag + 9Qz \quad (1)$$

$$5Hd + 3An + 4H_2O = 6Ttn + Fe - Act + Qz \quad (2)$$

$$2An + 8SiO_2 + 5Fe^{3+} + 4Na^{+} + Mg^{2+} + 4H_2O = Aeg - Aug + 2Ab + Fe_3O_4 + Ca^{2+} + 8H^{+} \quad (3)$$

involving oxidation and consumption of Fe-bearing pyroxene by fO_2 increase in the system (1), a pyroxene-plagioclase hydration reaction corresponding to lower fO_2 and to fH_2O increases in the system, with production of abundant titanite (2), and a more complex reaction of plagioclase and quartz with a Na - Mg – rich aqueous fluid (3). Conversely, with no Na excess the reaction (3) may also explain the early appearance of diopside.

The absence of ilmenite in the Sàrrabus studied rocks and the late segregation of titanite (or rather Al-OH titanite), involves reactions with consumption of anorthite component by hydration and oxidation (Harlov et al., 2006) according to the reaction:

$$24Hd + 12An + 2Mag + 18H_2O = 24Al - OH\ Ttn + 6Fe - Act + O_2 \quad (4)$$

Reaction (4) also involves the increase of fO_2 in the system, as commonly observed from the estimates of fO_2 according to the equation of Wones (1989) and Ridolfi (2021) (Table S7).

To estimate the chemical changes during metasomatism, we used the EASYGRESGRANT excel spreadsheet of López Moro (2012) based on the isocon method of Grant (1986). The model calculations are reported in Supplementary Material (Table S12). We estimate an unaltered starting composition similar to granodiorite sample SPP30 reported in Secchi et al. (2022) and an altered composition similar to episyenite SSP37 to simulate the early metasomatic processes (stage 1 in Fig. 13) forming the "leopard skin-like" episyenites. The isocon was defined using the cluster of slope method based on SiO_2, P_2O_5 and Eu as they behave consistently immobile in the episyenite. The calculated overall changes induced by the metasomatic event suggest a loss of 6.85% for the volume and a loss of 6.07% of the mass of the starting granodiorite.

Main variations for major elements involved a loss of K_2O (ΔCi of

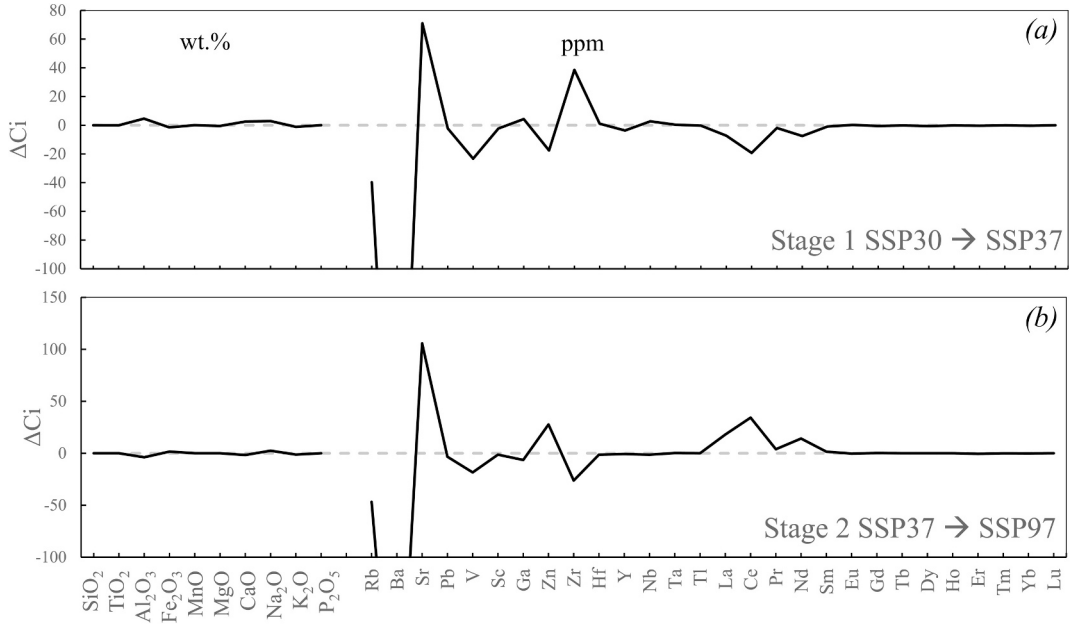

Fig. 13. results of mass balance calculation expressed as ΔCi (ΔCi is the change in concentration of species "i") for oxide major elements (Wt%) and trace elements (ppm) between the unaltered host granodiorite (data for sample SSP30 after Secchi et al., 2022) and selected episyenite (sample SSP37) for early stage metasomatism (*a*). Mass balance calculation for late stage metasomatism between episyenite SSP37 and SSP97 (*b*). Loss or gain for the respective components is reported as negative and positive values, respectively.

-1.2 wt%) in favor of CaO (ΔCi of 2.5 wt%) and Na_2O (ΔCi of 2.9 wt%) coupled to loss of Fe_2O_3 (ΔCi of -1.5 wt%) and enrichment in Al_2O_3 (ΔCi of 4.6 wt%) (Fig. 13a). Among trace elements the main variations comprehend loss of Rb (ΔCi of -39.7 ppm), Ba (ΔCi of -341.8 ppm) and LREE (La ΔCi of -7.3 ppm, Ce ΔCi of -19.3 ppm and Nd ΔCi of -7.5) (Fig. 13a) as expected during albitization processes (e.g. Kontonikas-Charos et al., 2014) while Sr (ΔCi of 71.05 ppm) and Zr (ΔCi of 38.6 ppm) increase.

A second model (Fig. 13b) was also made to simulate the late metasomatic stages producing xenomorphic or granoblastic episyenites starting from the composition of sample SSP37 as unaltered and the composition of sample SSP97 as altered. In this model SiO_2, TiO_2, MgO, Dy and Yb are considered immobile. The changes produced by the late metasomatic stages produced a loss of mass and volume of 3.33% from the starting material. Major elements variations suggest a loss of Al_2O_3 (ΔCi of -3.9 wt%), CaO (ΔCi of -1.7 wt%) and K_2O (ΔCi of -1.3 wt%) in favor of Fe_2O_3 (ΔCi of 1.6 wt%) and Na_2O (ΔCi of 2.4 wt%) (Fig. 13b). Trace elements show a loss for Ba (ΔCi of −328.0 ppm), Rb (ΔCi of -46.8 ppm), V (ΔCi of -18.46 ppm) and Zr (ΔCi of -26.2 ppm) in favor of Sr (ΔCi of 105.7 ppm), Zn (ΔCi of 27.7 ppm) and LREE (La ΔCi of 18.1 ppm, Ce ΔCi of 34.3 ppm and Nd ΔCi of 14.2) (Fig. 13b).

Overall, isoconic analyses with respect to hosting granodiorites suggests essential enrichments of Na, and minor Pb and Zr, on the contrary, Ca, K, minor Ti, Al, Mg and HREE depletion. Similar Sr and Nd isotopic signatures between albite-rich rocks and hosting granodiorites constrain the metasomatic fluids to a late-magmatic origin. The isocon model confirms that desilication process does not occur and it is recorded only locally with re-precipitation of quartz in veinlets as also observed in the *Q-P* diagram (Fig. 12).

6.7. Petrogenetic model for Sàrrabus episyenites

The whole data set indicates that the studied rocks are the product of alkali metasomatism of a granodioritic protolith, caused by rock-interaction with Na-enriched fluids at the boundaries of silica saturation, as suggested by low-Ti contents in andraditic garnets (Russell et al., 1999). Metasomatism proceeded through several stages into the still cooling granodioritic intrusion, controlled by extensional fault development and by continuous variations in physical and chemical characters of the fluids, under an overall decreasing temperature trend. Overall, high-temperature processes resulted in a singular "sodic fenite" stage, with coarse recrystallization textures and near-solidus recrystallization temperatures that overlap those of magmatic stage. This overlap is further confirmed by *P* values of 1.9 kbar, indistinguishable to that obtained for hosting granodiorites and related gabbroic rocks. High *T* textures are furtherly overlapped by decreasing temperature stages that favoured a general increase in Ca, fO_2 and aH_2O in the fluids, with a final and diffuse albitization which may be interpreted as a true episyenitization stage. The magmatic origin of metasomatizing fluid is confirmed by isotopic data and is coherent with coeval emplacement of granodioritic and gabbroic pulses along the SSSZ extensional shear zone (Secchi et al., 2021). With special regard to Campu Longu, our proposed petrogenetic model involves a component of alkaline fluids spreading from nearby gabbroic masses. Fluids could have been rapidly driven along the syn plutonic extensional shear zone where, under prevailing diffusive mechanisms focused in mechanically weakened zones. Under sub-magmatic conditions, alkaline fluids promoted the *HT* albitization of the magmatic feldspar framework ("sodic fenite" stage) in cooling granodiorites. Progressive recrystallization of Ca-rich mafic phases and titanite + magnetite, and albitization represent the final stage of the metasomatic process ("episyenite stage").

7. Conclusion

Field relationships and radiometric constraints suggest that Na-metasomatism observed in Sàrrabus pluton was coeval with the emplacement of the hosting granodiorites favoured by a tectonic setting dominated by an extensional stepover, which 1) drove the emplacement of several pulses of granodiorite magma, and 2) in a general regional uplift, favoured the Na-fluid exolution and flow. Geochronological data for the episyenite metasomatism obtained with U-Pb and Rb-Sr radiometric methods provide, within the correlated error, ages close to the host granodiorites and to the Monte Sette Fratelli which represent the younger intrusion of the pluton.

Several lines of evidence strongly support the granodioritic magma as the source of the metasomatizing fluids with no evidence for external – e.g., meteoric - fluids, as documented by chemical and Sr/Nd isotope systematics. Several calibrations constrain the *P–T–*fO_2 conditions at 1.9 kbar, 700–750 °C, and -18.5 – -16.2 bars, respectively.

Schematically, metasomatic stages may be bracketed into *HT* albitization and fluid-controlled multiple metasomatic reactions, direct precipitation of minerals from fluids, and a final widespread albitization with only local quartz reprecipitation in thin veinlets. Small aplo-pegmatitic bands, observed in some layered bodies, may be related to rapid cooling of a fluid-saturated residual granodioritic melt component, coeval to metasomatic processes.

Overall, the observed high-*T* metasomatic processes favoured the production of a "sodic fenite" with coarse recrystallization textures and near-solidus recrystallization temperatures overlapping those of host granodioritic stage.

CRediT authorship contribution statement

F. Secchi: Writing – review & editing, Writing – original draft, Supervision, Investigation, Funding acquisition, Data curation, Conceptualization. **S. Naitza:** Writing – review & editing, Writing – original draft, Conceptualization. **A.M. Conte:** Writing – review & editing, Validation, Investigation. **G. Oggiano:** Writing – review & editing, Writing – original draft. **M. Casalini:** Writing – review & editing, Validation, Investigation, Data curation. **M. Kohút:** Writing – review & editing, Writing – original draft. **T. Giovanardi:** Writing – review & editing, Writing – original draft, Validation, Investigation, Data curation, Conceptualization.

Declaration of competing interest

The authors declare that they have no known competing financial interests or personal relationships that could have appeared to influence the work reported in this paper.

Acknowledgements

This work was supported by DM737-SSCA-SECCHI and Fondo di Ateneo per la Ricerca -FAR2019- (Università di Sassari. Sassari, Italy). The study was also supported by Fondazione di Sardegna [S. Naitza, grant number CUP F23C25000090007 FDS 2023].

The Authors want to thank Daniel Miggins of the Oregon State University (Oregon, USA) for Ar-Ar helpful discussion and Leonardo Casini of the Università di Sassari for structural model discussion. The Authors would like to thank the editor and two reviewers for the discussions that helped to improve this article.

Appendix A. Supplementary data

Supplementary data to this article can be found online at https://doi.org/10.1016/j.lithos.2026.108674.

References

Akinfiev, N.N., Diamond, L.W., 2009. A simple predictive model of quartz solubility in water–salt–CO2 systems at temperatures up to 1000 °C and pressures up to 1000MPa. Geochim. Cosmochim. Acta 73 (6), 1597–1608. https://doi.org/10.1016/j.gca.2008.12.011.

Avanzinelli, R., Boari, E., Conticelli, S., Francalanci, L., Guarnieri, L., Perini, G., Petrone, C.M., Tommasini, S., Ulivi, M., 2005. High precision Sr, Nd, and Pb isotopic analyses using the new generation thermal Ionisation Mass Spectrometer ThermoFinnigan Triton-Ti®. Period. Miner. 74, 147–166.

Balia, R., Carrozzo, M.T., Loddo, M., Luzio, D., Margiotta, C., Quarta, T., Trudu, R., 1989. Carta Gravimetrica della Sardegna. Laboratorio di Cartografia ed editoria scientifica, Roma. https://doi.org/10.13140/RG.2.2.24140.92806.

Brotzu, P., Morbidelli, L., Traversa, G., 1978. Caratteri petrografici e chimici delle sieniti del Sarrabus meridionale (Sardegna sud-orientale). Period. Miner. 47, 83–98.

Brotzu, P., Ferrini, V., Masi, U., 1983. Stable isotope geochemistry of Hercynian granitoid rocks from the Sàrrabus massif (southeastern Sardinia, Italy). Isot. Geosc. 1, 77–90.

Brotzu, P., Callegari, E., Secchi, F., 1993. The search for the parental magma of the high-k alkaline igneous rock series in the southernmost Sardinia Batholith. Period. Mineral. 62, 253–280.

Cano, N., Camprubí, A., González-Partida, E., González-Ambrocio, A.K., Alfonso, P., Miggins, D.P., Fuentes-Guzmán, E., Cienfuegos-Alvarado, E., Iriondo, A., 2024. Metallogenic model of the Eocene Santa María and Antares Zn-Pb(-Ag) skarn deposits, Velardeña Mining District, Durango, Mexico. Miner. Deposita 59, 671–698. https://doi.org/10.1007/s00126-023-01225-4.

Carmignani, L., Carosi, R., Di Pisa, A., Gattigòlio, M., Musumeci, G., Oggiano, G., Pertusati, P.C., 1994. The hercynian chain in Sardinia (Italy). Geodin. Acta 7, 31–47. https://doi.org/10.1080/09853111.1994.11105257.

Carosi, R., Montomoli, C., Tiepolo, M., Frassi, C., 2012. Geochronological constraints on post-collisional shear zones in the Variscides of Sardinia (Italy). Terra Nova 24, 42–51. https://doi.org/10.1111/j.1365-3121.2011.01035.x.

Casini, L., Cuccuru, S., Maino, M., Oggiano, G., Puccini, A., Rossi, P., 2015a. Structural map of Variscan northern Sardinia (Italy). J. Maps 11, 1–10. https://doi.org/10.1080/17445647.2014.936914.

Casini, L., Cuccuru, S., Puccini, A., Oggiano, G., Rossi, Ph., 2015b. Evolution of the Corsica–Sardinia batholith and late-orogenic shearing of the Variscides. Tectonophysics 646, 65–78. https://doi.org/10.1016/j.tecto.2015.01.017.

Casini, L., Maino, M., Langone, A., Oggiano, G., Corvò, S., Reche-Estrada, J., Liesa, M., 2023. HTLP metamorphism and fluid-fluxed melting during multistage anatexis of continental crust (N Sardinia, Italy). J. Metam. Geol. 41 (1), 25–57. https://doi.org/10.1111/jmg.12687.

Cassano, E., Marcello, A., Nannini, R., Pretti, S., Ranieri, G., Salvaderi, R., Salvadori, I., 1979. Rilievo aeromagnetico della Sardegna e del mare circostante. Ente Minerario Sardo 3 (4), l-30.

Castorina, F., Masi, U., Padalino, G., Palomba, M., 2006. Constraints from geochemistry and Sr–Nd isotopes for the origin of albitite deposits from Central Sardinia (Italy). Miner. Deposita 41, 323–338. https://doi.org/10.1007/s00126-006-0049-7.

Charoy, B., Pollard, P.J., 1989. Albite-rich, silica-depleted metasomatic rocks at Emuford, Northeast Queensland: mineralogical, geochemical and fluid inclusion constraints on hydrothermal evolution and tin mineralization. Econ. Geol. 84, 1850–1874.

Cocherie, A., Rossi, Ph., Fanning, C.M., Guerrot, C., 2005. Comparative use of TIMS and SHRIMP for U-Pb zircon adting of A-type granites and mafic tholeiitic layered complexes and dykes from the Corsican Batholith (France). Lithos 82, 185–219.

Cocherie, A., Rossi, Ph., Fouillac, A.M., Vidal, Ph., 1994. Crust and mantle contributions to granite genesis -an example from the Variscan batholith of Corsica, France, studied by trace element and Nd-Sr-O-isotope systematics. Chem. Geol. 115, 173–211. https://doi.org/10.1016/0009-2541(94)90186-4.

Conte, A.M., Cuccuru, S., D'Antonio, M., Naitza, S., Oggiano, G., Secchi, F., Casini, L., Cifelli, F., 2017. The post-collisional late Variscan ferroan granites of southern Sardinia (Italy): Inferences for inhomogeneity of lower crust. Lithos 294-295, 263–282. https://doi.org/10.1016/j.lithos.2017.09.028.

Cuccuru, S., Naitza, S., Secchi, F., Puccini, A., Casini, L., Pavanetto, P., Linnemann, U., Hofmann, M., Oggiano, G., 2016. Structural and metallogenic map of late Variscan Arbus igneous complex (SW Sardinia, Italy). J. Maps 12, 860–865.

Cuney, M., Emetz, A., Mercadier, J., Mykchaylov, V., Shunko, V., Yuslenko, A., 2012. Uranium deposits associated with Na-metasomatism from Central Ukraine: A review of some of the major deposits and genetic constraints. Ore Geol. Rev. 44, 82–106. https://doi.org/10.1016/j.oregeorev.2011.09.007.

D'Angelo, R., 1998. Rilevamento e caratterizzazione petrografica delle masse basiche del settore Geremèas-Monte Turnu (Sàrrabus, Sardegna sud-orientale). M.Sc. Thesis. Università degli Studi di Cagliari, pp. 1–127.

Debon, F., Le Fort, P., 1988. A cationic classification of common plutonic rocks and åtheir magmatic associations: principles, method, applications. Bull. Minéral. 111, 493–510.

Desouky, M.E., Feely, M., Mohr, P., 1996. Diorite-granite magma mingling and mixing along the axis of the Galloway granite batholith Ireland. J. Geol. Soc. Lond. 153, 361–374.

Doi, N., Kato, T., Kubo, T., Ohnuma, S.R., Shimojuku, A., Suzuki, A., Ohtani, E., Kikegawa, T., 2009. Transformation experiment on sodium feldspar using deformation-cubic anvil, D-CAP 700, with synchrotron X-rays. In: American Geophysical Union Fall Meeting 2009. Abstract MR41A-1846.

Droop, G.T.R., 1987. A general equation for estimating Fe^{3+} concentrations in ferromagnesian silicates and oxides from microprobe analyses, using stoichiometric criteria. Mineral. Mag. 51, 431–435. https://doi.org/10.1180/minmag.1987.051.361.10.

Elliott, H.A.L., Wall, F., Chakhmouradian, A.R., Siegfried, P.R., Dahlgren, S., Weatherley, S., Finch, A.A., Marks, M.A.W., Dowman, E., Deady, E., 2018. Fenites associated with carbonatite complexes: a review. Ore Geol. Rev. 93, 38–59.

Erdmann, S., Wang, R., Huang, F., Scaillet, B., Zhao, K., Liu, H., Chen, Y., Faure, M., 2019. Titanite: a potential solidus barometer for granitic magma systems. Comptes Rendus. Géoscience 351, 551–561. https://doi.org/10.1016/j.crte.2019.09.002.

Franciosi, L., D'Antonio, M., Fedele, L., Guarino, V., Tassinari, C.C.G., de Gennaro, R., Cucciniello, C., 2019. Petrogenesis of the Solanas gabbro-granodiorite intrusion, Sàrrabus (southeastern Sardinia, Italy): implications for late Variscan magmatism. Int. J. Earth Sci. 108, 989–1012. https://doi.org/10.1007/s00531-019-01689-8.

Frezzotti, M.L., 1992. Magmatic immiscibility and fluid phase evolution in the Mount Genis granite (southeastern Sardinia, Italy). Geochim. Cosmochim. Acta 56, 21–33. https://doi.org/10.1016/0016-7037(92)90114-X.

Gaggero, L., Gretter, N., Langone, A., Ronchi, A., 2017. U–Pb geochronology and geochemistry of late Palaeozoic volcanism in Sardinia (southern Variscides). Geosci. Front. 8, 1263–1284. https://doi.org/10.1016/j.gsf.2016.11.015.

Grant, J.A., 1986. The isocon diagram; a simple solution to Gresens' equation for metasomatic alteration. Econ. Geol. 81, 1976–1982. https://doi.org/10.2113/gsecongeo.81.8.1976.

Grew, E.S., Locock, A.J., Mills, S.J., Galuskina, I.O., Galuskin, E.V., Hålenius, U., 2013. Nomenclature of the garnet supergroup. Am. Min. 25, 777–785. https://doi.org/10.2138/am.2013.4201.

Harlov, D., Tropper, P., Seifert, W., Nijland, T., Förster, H., 2006. Formation of Al-rich titanite ($CaTiSiO_4O$–$CaAlSiO_4OH$) reaction rims on ilmenite in metamorphic rocks as a function of fH_2O and fO_2. Lithos 88, 72–84. https://doi.org/10.1016/j.lithos.2005.08.005.

Hawthorne, F.C., Oberti, R., Harlow, G.E., Maresch, W.V., Martin, R.F., Schumacher, J.C., Welch, M.D., 2012. Nomenclature of the amphibole supergroup. Am. Mineral. 97, 2031–2048. https://doi.org/10.2138/am.2012.4276.

Hayden, L.A., Watson, E., Wark, D., 2008. A thermobarometer for sphene (titanite). Contrib. Mineral. Petrol. 155, 529–540. https://doi.org/10.1007/s00410-007-0256-y.

Holland, T., Blundy, J., 1994. Non-ideal interactions in calcic amphiboles and their bearing on amphibole-plagioclase thermometry. Contrib. Mineral. Petrol. 116, 433–447. https://doi.org/10.1007/BF00310910.

Kontonikas-Charos, A., Ciobanu, C.L., Cook, N.J., 2014. Albitization and redistribution of REE and Y in IOCG systems: Insights from Moonta-Wallaroo, Yorke Peninsula, South Australia. Lithos 208-209, 178–201. https://doi.org/10.1016/j.lithos.2014.09.001.

Koppers, A.A.P., 2002. ArArCALC—software for $^{40}Ar/^{39}Ar$ age calculations. Comput. Geosci. 28, 605–619. https://doi.org/10.1016/S0098-3004(01)00095-4.

Kuiper, K.F., Deino, A., Hilgen, F.J., Krijgsman, W., Renne, P.R., Wijbrans, A.J., 2008. Synchronizing rock clocks of earth history. Science 320 (5875), 500–504.

Le Bas, M.J., 2008. Fenites associated with carbonatites. Can. Mineral. 46, 915–932.

Leake, B.E., Woolley, A.R., Arps, C.E., Birch, W.D., Gilbert, M.C., Grice, J.D., Hawthorne, F.C., Kato, A., Kisch, H.J., Krivovichev, V.G., Linthouth, K., Laird, J., Mandarino, J.A., Maresch, W.V., Nickel, E.H., Rock, N.M.S., Schumacher, J.C., Smith, D.C., Stephenson, N.C.N., Ungaretti, L., Whittaker, E.J.W., Youzhi, G., 1997. Nomenclature of amphiboles; report of the subcommittee on amphiboles of the International Mineralogical Association, Commission on New Minerals and Mineral Names. Can. Mineral. 35 (1), 219–246.

Liao, Y., Wei, C., Rehman, H.U., 2021. Titanium in calcium amphibole: Behavior and thermometry. Am. Min. 106, 180–191. https://doi.org/10.2138/am-2020-7409.

Longerich, H.P., Jackson, S.E., Günther, D., 1996. Laser Ablation Inductively coupled Plasma Mass Spectrometric Transient Signal Data Acquisition and Analyte Concentration Calculation. J. Anal. At. Spectrom 11, 899–904. https://doi.org/10.1039/ja9961100899.

López Moro, F.J., 2012. EASYGRESGRANT—A Microsoft Excel spreadsheet to quantify volume changes and to perform mass-balance modeling in metasomatic systems. Comput. Geosci. 39, 191–196. https://doi.org/10.1016/j.cageo.2011.07.014.

Ma, Q., Evans, N.J., Ling, X.-X., Yang, J.-H., Wu, F.-Y., Zhao, Z.-D., Yang, Y.-H., 2019. Natural Titanite Reference Materials for in Situ U-Pb and Sm-Nd Isotopic Measurements by LA-(MC)-ICP-MS. Geostand. Geoanal. Res. 43 (3), 355–384. https://doi.org/10.1111/ggr.12264.

Macera, P., Di Pisa, A., Gasperini, D., 2011. Geochemical and Sm-Nd isotope disequilibria during multi-stage anatexis in a metasedimentary Hercynian crust. Eur. J. Mineral. 23, 207–222.

Martínez Catalán, J.R., Schulmann, K., Ghienne, J.F., 2021. The Mid Variscan Allochthon: keys from correlation, partial retrodeformation and plate-tectonic reconstruction to unlock the geometry of a non-cylindrical belt. Earth Sci. Rev. 220, 103700. https://doi.org/10.1016/j.earscirev.2021.103700.

McDonough, W.F., Sun, S.-S., 1995. The composition of the Earth. Chem. Geol. 120, 223–253. https://doi.org/10.1016/0009-2541(94)00140-4.

Meagher, E.P., 1982. Silicate garnets. In: Ribbe, P.H. (Ed.), Orthosilicates (Review in Mineralogy), 5. Mineralogical Society of America/Jahrbuch für Mineralogie, pp. 25–66.

Meloni, M.A., Oggiano, G., Funedda, A., Pistis, M., Linnemann, U., 2017. Tectonics, ore bodies, and gamma-ray logging of the Variscan basement, southern Gennargentu massif (Central Sardinia, Italy). J. Maps 13, 196–206.

Middlemost, E.A.K., 1994. Naming materials in the magma/igneous rock system. Earth Sci. Rev. 37, 215–224. https://doi.org/10.1016/0012-8252(94)90029-9.

Morimoto, N., 1989. Nomenclature of Pyroxenes. Can. Mineral. 27, 143–156. https://doi.org/10.2465/minerj.14.198.

Nishimoto, S., Yoshida, H., Asahara, Y., Tsuruta, T., Ishibashi, M., Katsuta, N., 2014. Episyenite formation in the Toki granite, Central Japan. Contrib. Mineral. Petrol. 167 (1), 960–971. https://doi.org/10.1007/s00410-013-0960-8.

Oggiano, G., Casini, L., Rossi, P., Mameli, P., 2007. Long lived dextral strike-slip tectonics in the southern Variscan Belt: evidences from two synkynematic intrusions of North Sardinia (Italy). Géol. Fr. 2, 142.

Paterson, S.R., Fowler, T.K., Schmidt, K.L., Yoshinobu, A.S., Yuan, E.S., Miller, R.B., 1998. Interpreting magmatic fabric patterns in plutons. Lithos 44, 53–82.

Pérez-Soba, C., Villaseca, C., 2019. Li-Na-metasomatism related to I-type granite magmatism: a case study of the highly fractionated La Pedriza pluton (Iberian Variscan belt). Lithos 344, 159–174. https://doi.org/10.1016/j.lithos.2019.06.008.

Petersson, J., Fallick, A.E., Broman, C., Eliasson, T., 2014. Imprints of multiple fluid regimes on episyenites in the Bohus granite, Sweden. Lithos 196-197, 99–114. https://doi.org/10.1016/j.lithos.2014.02.025.

Pirinu, N., 1994. Le sieniti del Sarrabus meridionale (Sardegna SE). Ph.D. Thesis, pp. 1–81. Napoli.

Pirinu, N., Brotzu, P., Callegari, E., Secchi, F., 1996. Age and field relationships of albite-rich mozosyenite intruded into the Sàrrabus granitoids (SE Sardinia, Italy). Per. Mineral. 63, 239–304.

Poli, G., Tommasini, S., 1999. Geochemical modelling of acid-basic magma interaction in the Sardinia-Corsica batholith: the case study of Sàrrabus, south easterns Sardinia, Italy. Lithos 46 (3), 553–571. https://doi.org/10.1016/S0024-4937(98)00082-6.

Pouchou, J.L., Pichoir, F., 1991. Quantitative Analysis of Homogeneous or Stratified Microvolumes applying the Model "PAP". In: Heinrich, K.F.J., Newbury, D.E. (Eds.), Electron Probe Quantification. Plenum Press, New York, pp. 31–75. https://doi.org/10.1007/978-1-4899-2617-3_4.

Ridolfi, R., 2021. Amp-TB2: an updated model for calcic amphibole thermobarometry. Minerals 11, 324. https://doi.org/10.3390/min11030324.

Rizzo, R., 1994. Prospezione geomineraria per minerali di Terre Rare in rocce albititiche associate ai granitoidi della Sardegna. Ph.D. Thesis. Università degli Studi di Cagliari, pp. 1–574.

Ronca, S., Del Moro, A., Traversa, G., 1999. Geochronology, Sr-Nd isotope geochemistry and petrology of late Hercynian dike magmatism from Sarrabus (SE Sardinia). Period. Mineral. 68, 231–260.

Rossi, Ph., Cocherie, A., Fanning, C.M., 2015. Evidence in Variscan Corsica of a brief and voluminous late Carboniferous to early Permian volcanic-plutonic event contemporaneous with a high-temperature/low-pressure metamorphic peak in the lower crust. Bull. Soc. Geol. Fr. 186, 171–192. https://doi.org/10.2113/gssgfbull.186.2-3.171.

Russell, J.K., Dipple, G., Lang, J., Lueck, B., 1999. Major-element discrimination of titanian andradite from magmatic and hydrothermal environments: an example from the Canadian Cordillera. Eur. J. Mineral. 11, 919–935. https://doi.org/10.1127/ejm/11/6/0919.

Secchi, F., Naitza, S., Oggiano, G., Cuccuru, S., Puccini, A., Conte, A.M., Giovanardi, T., Mazzucchelli, M., 2021. Geology of late-Variscan Sàrrabus pluton (South-Eastern Sardinia, Italy). J. Maps 17, 591–606. https://doi.org/10.1080/17445647.2021.1982032.

Secchi, F., Giovanardi, T., Naitza, S., Casalini, M., Kohút, M., Conte, A.M., Oggiano, G., 2022. Multiple crustal and mantle inputs in post-collisional magmatism: evidence from late-Variscan Sàrrabus pluton (SE Sardinia, Italy). Lithos 420-421, 106697. https://doi.org/10.1016/j.lithos.2022.106697.

Shearer, C.K., Larsen, L.M., 1994. Sector-zoned aegirine from the Ilimaussaq alkaline intrusion, South Greenland: implications for trace-element behavior in pyroxene. Am. Mineral. 79, 340–352.

Shoji, T., 1978. Phase relations in the system CaO-FeO_x-SiO_2 in H_2O-CO_2 mixtures. J. Japan. Assoc. Min. Petr. Econ. Geol. 73, 231–240.

Suikkanen, E., Rämö, T., 2019. Episyenites—characteristics, genetic constraints and mineral potential. Min. Metall. Explor. 36 (5), 861–878. https://doi.org/10.1007/s42461-019-00120-9.

Sun, S., McDonough, W.F., 1989. Chemical and isotopic systematics of oceanic basalts: implications for mantle composition and processes. In: Geological Society, London, Special Publications, 42, pp. 313–345. https://doi.org/10.1144/GSL.SP.1989.042.01.19.

Thirlwall, A.P., 1991. The absolute isotopic abundance ratios of strontium—$^{87}Sr/^{86}Sr$. Chem. Geol. 94 (3–4), 349–356. https://doi.org/10.1016/j.palaeo.2007.02.028.

Tommasini, S., Poli, G., Halliday, A.N., 1995. The role of sediment subduction and crustal growth in Hercynian plutonism: isotopic and trace element evidence from the Sardinia–Corsica Batholith. J. Petrol. 36, 1305–1332.

Vartiainen, H., Woolley, A.R., 1976. The petrography, mineralogy and chemistry of the fenites of the Sokli carbonatite intrusion, Finland. Geol. Surv. Finland Bull. 280, 1–87.

Vermeesch, P., 2018. IsoplotR: a free and open toolbox for geochronology. Geosci. Front. 9, 1479–1493. https://doi.org/10.1016/j.gsf.2018.04.001.

Warr, L.N., 2021. IMA–CNMNC approved mineral symbols. Mineral. Mag. 85, 291–320. https://doi.org/10.1180/mgm.2021.43.

Wones, D.R., 1989. Significance of the assemblage titanite + magnetite + quartz in granitic rocks. Am. Mineral. 74, 744–749.

Zharikov, V.A., Pertsev, N.N., Rusinov, V.L., Callegari, E., Fettes, D.J., 2007. Metasomatism and metasomatic rocks. In: Recommendations by the IUGS Subcommission on the Systematics of Metamorphic Rocks. Online Document. http://www.bgs.ac.uk/scmr/docs/papers/paper_9.pdf. Accessed date: 23 June 2017.